PCCP

PAPER

Cite this: *Phys. Chem. Chem. Phys.*, 2019, **21**, 3453

Rovibrational quantum dynamics of the vinyl radical and its deuterated isotopologues

Jan Šmydke, [a] Csaba Fábri, [a] János Sarka [b] and Attila G. Császár *[a]

Received 23rd July 2018,
Accepted 22nd October 2018

DOI: 10.1039/c8cp04672g

rsc.li/pccp

Rotational–vibrational states up to 3200 cm^{-1}, beyond the highest-lying stretching fundamental, are computed variationally for the vinyl radical (VR), $H_2C_\beta{=}C_\alpha H$, and the following deuterated isotopologues of VR: $CH_2{=}CD$, $CHD{=}CH$, and $CD_2{=}CD$. The height of the $C_\alpha H$ tunneling rocking barrier of VR, partially responsible for the complex nuclear dynamics of VR and its isotopologues, is determined to be 1641 ± 25 cm^{-1} by the focal-point analysis approach. The definitive nuclear-motion computations performed utilize two previously published potential energy hypersurfaces and reveal interesting energy-level and tunneling patterns characterizing the internal motions of the four isotopologues. A full assignment, including symmetry labels, of the vibrational states computed for $CH_2{=}CH$ is provided, whenever feasible, based on the analysis of wave functions and the related one- and two-mode reduced density matrices. The computed vibrational states of $CH_2{=}CD$ and $CD_2{=}CD$ are characterized up to slightly above the top of the barrier. Interestingly, it is the interplay of the ν_6 (formally CH_2 rock) and ν_7 (formally CH rock) modes that determines the tunneling dynamics; thus, the description of tunneling in VR needs, as a minimum, the consideration of two in-plane bending motions at the two ends of the molecule. When feasible, the computed results are compared to their experimental counterparts as well as to previous computational results. Corrections to the placement of the ν_4 and ν_6 fundamentals of VR are proposed. Tunneling switching, a unique phenomenon characterizing tunneling in slightly asymmetric effective double-well potentials, is observed and discussed for $CHD{=}CH$. Despite the extensive tunneling dynamics, the rotational energy-level structure of VR exhibits rigid-rotor-type behavior.

1 Introduction

The vinyl radical (VR), $H_2C_\beta{=}C_\alpha H$ (see Fig. 1 and 2), the simplest open-shell olefinic radical, plays an important role in combustion chemistry,[1,2] mostly as a short-lived reactive intermediate, in plasma chemistry,[3] and in the chemistry of planetary atmospheres.[4] Besides these important contributions of VR to interesting fields of chemistry, the structure and the internal motions of the radical, involving several possible tunneling pathways, are also of considerable interest in their own right.

Consequently, the structure, the (ro)vibrational quantum dynamics, and the related (high-resolution) spectra of VR on its $\tilde{X}^2A'$ ground electronic state surface have been the subject of a considerable number of experimental (spectroscopic)[5–24] and computational (quantum chemical)[25–40] investigations. Furthermore, although of no direct relevance for the present study, we note that vibrational transitions between several electronic states of VR have also been studied experimentally.[9,41–45]

Through the magnitude of the observed inertial defects associated with the ground-state rotational constants determined, Hirota *et al.*[11] clearly established experimentally that the equilibrium structure of VR on its $\tilde{X}^2A'$ surface has a plane of symmetry. From the observed splitting of the CH_2 wagging mode (ν_8) at about 895 cm^{-1} and the consideration of the associated nuclear spin statistical weights, Hirota *et al.*[11] deduced that the structure of VR has an effective C_{2v} point-group symmetry, corresponding to a transition state along the tunneling rocking motion of $C_\alpha H$ between two equivalent C_s minima, as shown in Fig. 1. An experimental estimate of the effective (ground-state) structure of VR was also derived by Hirota *et al.*,[11] based on the effective rotational constants they measured. By fixing four of the seven independent structural parameters of VR, the three CH bond lengths and the $C_\alpha C_\beta H$ bond angle, at reasonable values, they obtained 1.3160(63) Å and 137.3(40)° for the C=C bond length and the $C_\beta C_\alpha H$ bond angle, respectively. Later, by a similar analysis of the measured inertial defects, Tanaka *et al.*[15] suggested that the C=C bond length is 1.314(4) Å and the $C_\beta C_\alpha H$ angle is 138.3(20)° (see Table 1). Clearly, even the latter structural parameters have unacceptably

[a] *MTA-ELTE Complex Chemical Systems Research Group and Laboratory of Molecular Structure and Dynamics, Institute of Chemistry, ELTE Eötvös Loránd University, H-1117 Budapest, Pázmány Péter sétány 1/A, Hungary. E-mail: csaszarag@caesar.elte.hu*

[b] *Department of Chemistry and Biochemistry, Texas Tech University, Lubbock, Texas 79409, USA*

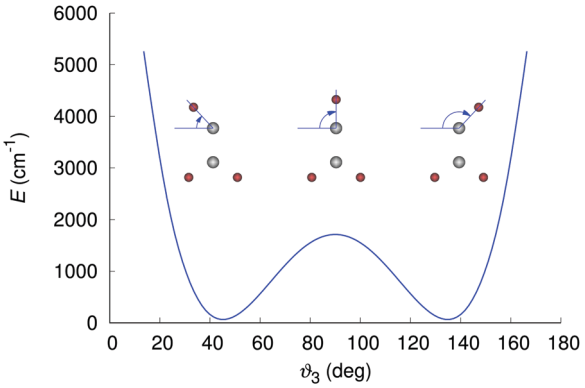

Fig. 1 The one-dimensional potential energy curve hindering the $C_\alpha H$ rocking motion in the vinyl radical, $H_2C_\beta{=}C_\alpha H$, leading to tunneling behavior. The rocking internal coordinate ϑ_3 (see Fig. 2 for its definition) mimics the assumed one-dimensional tunneling path. The three stationary-point structures involved in the rocking tunneling motion over a symmetric double-well potential are indicated using grey and red balls corresponding to the C and H atoms, respectively.

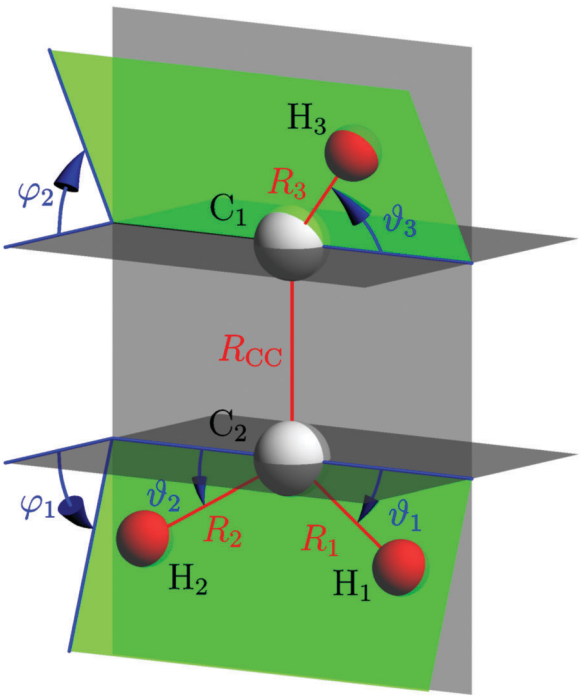

Fig. 2 Definition of the internal coordinate system employed in this study for describing the internal motions of the vinyl radical.

large uncertainties; present-day sophisticated electronic structure computations can yield considerably more reliable estimates of the bond lengths and especially the bond angles for small and well-behaved semirigid molecules.[46,47]

As demonstrated by the data of Table 1, electronic structure computations yield an equilibrium structure for VR in its $\tilde{X}^2A'$ state having C_s point-group symmetry and a $C_\alpha H$ rocking tunneling transition state (TS) structure of C_{2v} point-group symmetry. Variation of the structural parameters obtained at the different levels of theory does not exceed what one would expect and can be ascribed as the uncertainty of the computed results.

As to the internal motions of VR, the spectroscopic observations are characterized by several peculiarities. These peculiarities help explain why VR has become one of the favorite targets of experimental (and quantum chemical) nuclear dynamics investigations. For example, VR is a member of the exceedingly small class of polyatomic molecules for which nuclear spin isomer conversion has been measured and conversion rates established.[20,48]

If the assumed TS of the proton tunneling motion characteristic of VR is of C_{2v} point-group symmetry (confirmed by electronic-structure computations, see Table 1), the two $C_\beta H$ protons are equivalent and the tunneling is described as a $C_\alpha H$ rocking tunneling. Then, nuclear-spin (proton-spin) statistics suggest that the spectrum should show the usual 1 : 3 intensity alternation of the related transitions of the *ortho*- and *para*-VR molecules. This is equivalent to saying that the intensity alternation is 1 : 3 for the even : odd K_a levels. This type of intensity alternation has indeed been observed for the ν_8 mode of VR by Hirota *et al.*,[11] who measured a band splitting of 0.0541(11) cm^{-1} for ν_8 (see Table 2). Unexpectedly, Nesbitt *et al.*,[18] when they studied the splitting of the ν_3 mode, observed cases with no intensity alternation in the spectrum. One possible explanation is that in this case the three protons of VR become "equivalent", resulting in a 4 : 4 intensity ratio. This observation can be attributed to the high vibrational excitation of the radical due to dissociative electron attachment in the discharge. To produce vinyl radicals subsequently captured by He droplets, Douberly *et al.*[23] used a pyrolysis source. Since the pyrolysis temperature was about 1500 K, the equilibrium temperature of the vinyl radicals prior to droplet pick-up should be similarly high, whereby H-atom scrambling occurs. The spectroscopic results of Douberly *et al.*[23] are consistent with a 4 : 4 nuclear spin weight ratio for even : odd K_a levels in the ground state. The computations of Sharma, Bowman, and Nesbitt[38] confirm that a large-amplitude tunneling over a high barrier (*ca.* 20 000 cm^{-1}) from vibrationally excited states is realistic at relatively low temperatures of $T > 1300$ K. Nesbitt *et al.*[18] could also observe a spectral feature in the ν_3 band which showed the "expected" 1 : 3 intensity ratio. As explained later by Douberly *et al.*,[23] the "anomalous $\approx$3 : 1 intensity ratio observed in the jet-cooled spectrum for the ν_3^+ and ν_3^- bands indicates a tunneling manifold dependent oscillator strength for the CH_2 symmetric stretch". Finally, Tanaka *et al.*[20] predicted fast *ortho–para* conversion due to nuclear and electron spin interactions and the proximity of the *ortho* and *para* rotational states because of tunneling doubling (*vide infra*). Enhanced conversion rates were also measured for $H_2C{=}CD$ and $D_2C{=}CD$.[20,24]

The 1 : 3 intensity ratio depends critically on the equivalence of the two H_β nuclei. If they are non-equivalent for some reason, at least on the timescale of the experiment, the splitting pattern and the intensity alternation can change dramatically. This non-equivalence can be achieved by a non-symmetric deuteration, the case of the $CHD{=}CH$ species. This deuterated isotopomer of VR is also of interest as it should provide another

Table 1 Optimized geometry parameters of the minimum (C_s point-group symmetry) and transition state (C_{2v} point-group symmetry) structures of the vinyl radical on its $\tilde{X}^2A'$ ground electronic state surface. See Fig. 2 for the definition of the coordinates. The internuclear distances are in Å, the angles are in degrees, and $\varphi_1 = \varphi_2 = 90^\circ$ both for the minimum and the transition state

Stationary point	Method/basis	R_{CC}	R_1	R_2	R_3	ϑ_1	ϑ_2	ϑ_3	Ref.
Minimum	CCSD(T)/TZ2P	1.314	1.088	1.083	1.078	31.2	31.3	46.6	29
	CCSD(T) + corrections/cc-pVQZ	1.3102	1.0881	1.0830	1.0773	31.3	32.0	47.0	31
	UCCSDT/CBS	1.3082	1.0885	1.0829	1.0772	31.24	32.09	47.04	33
	CCSD(T)/AVQZ	1.3138	1.0901	1.0845	1.0788	31.205	31.994	47.068	35
	UCCSD(T)-F12a/aug-cc-pVTZ[a]	1.3123	1.0904	1.0849	1.0779	31.358	32.023	47.454	39
	ROCCSD(T)/aug-cc-pCVQZ[b]	1.3107	1.0888	1.0832	1.0773	31.232	32.031	47.180	
	UCCSD(T)/aug-cc-pwCVQZ[b]	1.3078	1.0886	1.0831	1.0772	31.228	32.054	47.214	
	Experiment	1.3160(63)						47.3(40)	11
	Experiment	1.314(4)						48.3(20)	15
Transition state	CCSD(T)/TZ2P	1.304	1.089	1.089	1.064	32.2	32.2	90.0	29
	CCSD(T)/AVQZ	1.3038	1.0912	1.0912	1.0652	32.221	32.221	90.0	35
	UCCSD(T)-F12a/aug-cc-pVTZ[a]	1.3037	1.0908	1.0908	1.0645	32.233	32.233	90.0	39
	ROCCSD(T)/aug-cc-pCVQZ[b]	1.3009	1.0899	1.0899	1.0639	32.260	32.260	90.0	
	UCCSD(T)/aug-cc-pwCVQZ[b]	1.2981	1.0898	1.0898	1.0636	32.236	32.236	90.0	

[a] The values correspond to the geometries of the stationary points optimized on the $H_{1,2}$-symmetrized NN-PES.[39] [b] All-electron computations, this work.

example of the tunneling switching behavior,[49–51] studied *via* high-resolution spectroscopy by Quack *et al.*[51] for a molecule as large as phenol and its *meta*-D substituted analogue. Tunneling switching is an interesting dynamical phenomenon characterizing slightly asymmetric effective double-well potentials and can be easily understood by a simple two-state model.[49]

A major goal of the present study is to provide accurate variational rovibrational results for VR and three of its deuterated isotopologues to explore further the mentioned interesting tunneling phenomena. Furthermore, conflicting statements in the literature about some spectral features of VR, detailed below, also call for more definitive studies on VR.

While there are several reports[13,16,19,21,23,35,44] about the determination of the vibrational fundamentals of VR, they do not seem to agree with each other sufficiently well, as detailed in Table 2. The exception is the CH stretch region. Here, fairly elaborate measurements have been done by the group of Douberly,[23] who trapped VR in ^{4}He nanodroplets and probed the region between 2850 and 3200 cm^{-1} *via* infrared (IR) laser spectroscopy. They measured a number of transitions within the ν_1 (C_αH stretch), ν_2 (as-CH_2 stretch), and ν_3 (s-CH_2 stretch) bands and successfully explained most of the measured spectral features. The jet-cooled results of Nesbitt *et al.*[18] also fully support the position of the ν_3 band. As a result, these three fundamentals of VR appear to be very well established. Nevertheless, unusually for such a small molecule, most of the remaining fundamentals of VR are not known with the same certainty. In the lower-frequency region the available experimental results are a lot more disparate; especially problematic is a time-resolved Fourier-transform infrared (FTIR) emission spectroscopy study of Letendre *et al.*[13] This study resulted in consistently too high fundamental values, disagreeing with most other experimental sources by more than 100 cm^{-1} (the same holds for the CH-stretch region). The conflict between this experiment and theory for the ν_5 mode of VR has been discussed by Sattelmeyer and Schaefer.[32] Some further misassignments seem to hinder further the full understanding of the internal dynamics of VR.

Understanding the effect of the tunneling motion of VR on all the fundamentals as well as the combination and overtone bands is also of considerable interest. As shown by a couple of examples,[52–54] tunneling can be enhanced as well as inhibited by different nuclear motions.

The most important features on the PES of VR are related to two tunneling pathways, the short C_αH and the long C_βH ones. The barrier to the C_αH rocking tunneling motion is relatively low. Thus, the facile C_αH rocking tunneling motion leads to appreciable splittings of the rovibrational states. This motion necessitates the use of the $C_{2v}(M) = S_2^*$ molecular symmetry (MS) group[55] for the characterization of the lower-lying rovibrational states of VR. If scrambling of all three hydrogens of VR was feasible and observable, one would need to use the S_3^* MS group. While explaining the observed doublets in their electron-spin-resonance (ESR) experiments, Fessenden and Schuler[5] estimated that the barrier hindering the C_αH rocking motion of VR cannot be lower than 700 cm^{-1}. Later, Hirota *et al.*[11] suggested that an energy barrier of 1200 cm^{-1} would reproduce best their observed data, the difference between the tunneling splitting of 0.0541 cm^{-1} in the ν_8 absorption band at about 895 cm^{-1} (see Table 2). Even later, Tanaka *et al.*[15] measured accurately the ground-state tunneling splitting by millimeter wave (MMW) spectroscopy and obtained a value of 0.5427702(2) cm^{-1}. Analyzing a 1-dimensional (1D) tunneling model, they estimated the effective barrier to be 1580 cm^{-1}, noting that the model was highly sensitive to the supplied $C_\beta C_\alpha$H angle and thus the associated uncertainty may be more than 100 cm^{-1}. As to the computational results concerning this barrier, Wang *et al.*[29] computed its height at the CCSD(T) level using various basis sets up to TZ2P quality and the results scattered between 1672 and 2195 cm^{-1}. Mil'nikov *et al.*[34] used instanton theory to study the C_αH tunneling and the electronic barrier was estimated to be

Table 2 Collection of measured and some computed anharmonic vibrational fundamentals ($\tilde{\nu}_i$) and the corresponding tunneling splittings ($\Delta\tilde{\nu}_i = \tilde{\nu}_i^- - \tilde{\nu}_i^+$) of CH_2=CH. All values are in cm^{-1}

Mode	$\tilde{\nu}_i$	$\Delta\tilde{\nu}_i$	Comments
$\nu_1(a')$	3235(12)		Time-resolved FTIR emission spectroscopy[13]
	3064.6	0.31	Vibrationally adiabatic approach[35,a]
	3141.0		Infrared absorption spectrum in solid Ne[19]
	3108.4		VCI on a CCSD(T)/aug-cc-pVTZ PES[36]
	3119.6263(1)	0.44	IR spectroscopy in He nanodroplets[23]
	3120.5	0.68	Full-dimensional variational[40]
$\nu_2(a')$	3164(20)		Time-resolved FTIR emission spectroscopy[13]
	3018.2	0.30(2)	IR spectroscopy in He nanodroplets[23]
	3000.7	0.70	Vibrationally adiabatic approach[35,a]
	2953.6		Infrared absorption spectrum in solid Ne[19]
	3015.9		VCI on a CCSD(T)/aug-cc-pVTZ PES[36]
	3022.5	0.36	Full-dimensional variational[40]
$\nu_3(a')$	3103(11)		Time-resolved FTIR emission spectroscopy[13]
	2904.020	0.50(1)	IR spectroscopy in He nanodroplets[23]
	2901.8603(7)	0.6144(5)	Jet-cooled hi-resolution infrared spectroscopy[18]
	2901.9	0.62	Vibrationally adiabatic approach[35,a]
	2911.5		Infrared absorption spectrum in solid Ne[19]
	2900.7		VCI on a CCSD(T)/aug-cc-pVTZ PES[36]
	2903.7	0.19	Full-dimensional variational[40]
$\nu_4(a')$	1700(35)		Time-resolved FTIR emission spectroscopy[13]
	1522.1	0.55	Vibrationally adiabatic approach[35,a]
	1595(10)		Time-resolved IR emission spectroscopy[21]
	1632	106	Instanton theory[34]
	1583.6	0.76	Full-dimensional variational[40]
$\nu_5(a')$	1277(20)		Time-resolved FTIR emission spectroscopy[13]
	1401(5)		Time-resolved IR emission spectroscopy[21]
	1359.7		Infrared spectra in solid Ne[22]
	1357.4		IR absorption spectrum in solid Ne[19]
	1356.7		Ar matrix[16] (Kr matrix: 1353.2, Xe matrix: 1348.9)[16]
	1314.5	0.50	Vibrationally adiabatic approach[35,a]
	1390	9.01	Instanton theory[34]
	1357.8	1.58	Full-dimensional variational[40]
$\nu_6(a')$	1099(16)		Time-resolved FTIR emission spectroscopy[13]
	1074(8)		Time-resolved IR emission spectroscopy[21]
	1007.3	0.90	Vibrationally adiabatic approach[35,a]
	1062	1.59	Instanton theory[34]
	996.3	13.7	Full-dimensional variational[40]
$\nu_7(a')$	895(9)		Time-resolved FTIR emission spectroscopy[13]
	674(2)		Vibrationally resolved electronic spectra[44]
	677.1		Infrared absorption spectra in solid Ne[19]
	677.0		Infrared spectra in solid Ne[22]
	711	19.1	Instanton theory[34]
	667.5	13.9	Full-dimensional variational[40]
$\nu_8(a'')$	900		FTIR in solid Ar[10]
	895.1625(4)	0.597(1)	IR diode laser kinetic spectroscopy[11]
	895.4		IR spectroscopy in solid Ne[12]
	944(6)		Time-resolved IR emission spectroscopy[21]
	955(7)		Time-resolved FTIR emission spectroscopy[13]
	900.8		Ar matrix[16] (Kr matrix: 896.6, Xe matrix: 891)[16]
	858.1	0.55	Vibrationally adiabatic approach[35,a]
	895.3		IR absorption spectra in solid Ne[19]
	897.4		IR spectra in solid Ne[22]
	923	0.68	Instanton theory[34]
	889.7	0.65	Full-dimensional variational[40]
$\nu_9(a'')$	758(5)		Time-resolved FTIR emission spectroscopy[13]
	756.5	0.80	Vibrationally adiabatic approach[35,a]
	857.0		IR absorption spectra in solid Ne[19]
	897(6)		Time-resolved IR emission spectroscopy[21]
	813	1.17	Instanton theory[34]
	755.1	2.08	Full-dimensional variational[40]

Table 2 (*continued*)

Mode	$\tilde{\nu}_i$	$\Delta\tilde{\nu}_i$	Comments
GS		0.5427702(2)	MMW spectroscopy[15]
		0.46	Vibrationally adiabatic approach[35]
		0.43	Reduced dimensional approach[37]
		0.41(1)	IR spectroscopy in He nanodroplets[23]
		0.53	Instanton theory[34]
		0.53	Full-dimensional variational[40]

[a] CCSD(T)/CBS potential scaled to match the GS tunneling splitting of 0.5428 cm^{-1}, measured by Tanaka *et al.*[15]

1770 cm^{-1} at the CCSD(T)/aug-cc-pVTZ level. Bowman *et al.*[36] reported the value of 1754 cm^{-1} for the electronic barrier employing the CCSD(T)/aug-cc-pVTZ level of electronic structure theory. Nesbitt and Dong[35] used a vibrationally adiabatic 1D potential, obtained at the CCSD(T)/CBS level, where CBS means complete basis set limit, and accounted for the zero-point vibrational energy (ZPVE) contributions of the remaining vibrational coordinates. The barrier they obtained, 1763(20) cm^{-1}, resulted in a too small splitting of the ground vibrational state. They then scaled the 1D potential down to match the computed splitting with the observed[15] one. This procedure led to an empirically improved barrier of 1696(20) cm^{-1}. When the potential was further corrected for the zero-point energy contribution, the effective tunneling barrier became 1602(20) cm^{-1}. Since the literature data mentioned do not provide a highly accurate estimate for the $C_\alpha H$ rocking tunneling barrier corrected for vibrational motions, the focal-point analysis (FPA) technique[56–58] has been employed in this study to compute an accurate tunneling barrier for VR (*vide infra*). The corresponding double-well potential is shown in Fig. 1.

At this point it is necessary to return to the feasibility of the complete scrambling of the hydrogens of VR. The H migration between the two carbon atoms ($C_\beta H \rightarrow C_\alpha H$) leads either to a symmetrically equivalent vinyl radical *via* different transition states[25,29,36,38] or to isomerization to the methylcarbyne molecule.[36,59] The barrier heights involved in these motions are, however, an order of magnitude larger than that hindering the $C_\alpha H$ rocking tunneling motion: Harding[25] estimated the H migration barrier to be 57 kcal mol^{-1}, *i.e.*, 19 900 cm^{-1}, Wang *et al.*[29] predicted it to be at least 47 kcal mol^{-1}, *i.e.*, 16 400 cm^{-1}, while Bowman *et al.*[36] computed 17 756 cm^{-1} for a non-planar saddle point, 17 869 cm^{-1} for a planar saddle point, and 19 685 cm^{-1} for an isomerization transition state to the methylcarbyne local minimum. Therefore, the motions through these exceedingly large barriers are not considered further in the present study as not only the barriers are high but the tunneling motions would have a very long path, preventing efficient and thus readily observable tunneling.

As mentioned above, Tanaka *et al.*[15] identified a number of pure rotational and rotational-tunneling transitions in the MMW spectrum of VR and determined the ground vibrational state splitting to be 0.5427702(2) cm^{-1}. Some of the deuterated isotopologues of VR were also investigated by Tanaka and co-workers[20] by MMW spectroscopy and there the ground-state splittings were found to be an order of magnitude smaller, 0.0395871(5) and 0.0257507(6) cm^{-1} for $H_2C{=}CD$ and $D_2C{=}CD$, respectively (see Table 3, containing also the measured fundamentals of these molecules). We are not aware of splittings of other rovibrational states determined for the deuterated isotopologues of VR experimentally.

As to the dynamical models used for the description of the tunneling dynamics of VR, Tanaka *et al.*[15] employed a 1D model and used it to estimate the $C_\alpha H$ tunneling barrier height. The theoretical studies also employed instanton theory,[34] vibrationally adiabatic 1D models,[35] and a reduced-dimensional approach.[37] It was only in 2017 that Yu *et al.*[40] reported a full-dimensional description of the tunneling motion of VR. They determined the vibrational eigenstates for all fundamentals and provided splittings also for the excited vibrational states for $CH_2{=}CH$. A summary of the measured and computed tunneling splittings of the fundamental modes of VR is given in Table 2. There are also a few experimental studies concerning the vibrations of the various ^{13}C and deuterated VR isotopologues.[10,14,16,19–22,24,44]

Table 3 Experimental values of the fundamental modes and the ground-state splitting, in cm^{-1}, for the $CH_2{=}CD$ and $CD_2{=}CD$ molecules

Mode	$CH_2{=}CD$	$CD_2{=}CD$	Comments
$\nu_1(a')$		2348.0	IR in solid Ne[19]
$\nu_2(a')$		2192.5	IR in solid Ne[19]
$\nu_3(a')$		2124.1	IR in solid Ne[19]
$\nu_5(a')$		996.5	IR and EPR in Kr matrix[16]
		993.8	IR and EPR in Xe matrix[16]
		1000.4	IR in solid Ne[19]
		1060(15)	Time-resolved IR emission[21]
		1002.1	IR in Ne[22]
$\nu_6(a')$		820(6)	Time resolved IR emission[21]
$\nu_8(a'')$	887	704	FTIR in solid Ar[10]
	883.8	701.7	IR and EPR in Kr matrix[16]
	879.5	698.9	IR and EPR in Xe matrix[16]
		704.8	IR in solid Ne[19]
		728(9)	Time-resolved IR emission[21]
		705.2	IR in Ne[22]
$\nu_9(a'')$		654.5	IR in solid Ne[19]
		612.2	IR in Ne[22]
GS[a]		>0.01	FTMW[14]
	0.0395871(5)	0.0257507(6)	MMW[20]
	0.03960		MMW[24]

[a] Tunneling splitting of the ground vibrational state.

Given all the previous experimental and computational work discussed above, in this study we decided to focus on the $C_\alpha H$ tunneling dynamics of four isotopologues of VR: $CH_2{=}CH$, $CH_2{=}CD$, $CHD{=}CH$, and $CD_2{=}CD$. These isotopologues have been chosen as they help explain different observations and guide future experiments.

Performing variational nuclear-motion computations in full dimensions for a five-atom molecule with 12 internal degrees of freedom including large-amplitude motions still offers considerable technical challenges. In this study we compare two feasible approaches applied to the computation of vibrational eigenstates. One is a full-dimensional conventional computation on a direct-product (either simple or symmetry-adapted) grid. The other is a contracted scheme, in which two complementary reduced-dimensional problems (in the simplest case the separation of the stretching and bending subspaces, which usually have about the same number of internal degrees of freedom) are solved separately first and then the full-dimensional Hamiltonian is constructed in a direct product basis of the eigenstates of the two subproblems. The latter approach may make the computation of even larger systems feasible, but it is not yet clear within our variational approach how well the contraction results converge towards the conventionally computed eigenvalues with the increase in the basis size of the two subspaces and what the computational bottlenecks are. Along the way we are computing all the vibrational states of $CH_2{=}CH$ up to the highest-lying CH stretch fundamental. Due to our symmetry-adapted nuclear-motion computations[60] it is straightforward for us to attach symmetry labels, including parity, to all the computed vibrational states, contributing substantially to their theoretical characterization. Employing one- and two-mode reduced density matrices, we provide not only well-established symmetry labels but also internal motion labels to all the computed vibrational states. We also investigate whether the large-amplitude tunneling motion would result in unusual rovibrational characteristics.

2 Computational details

2.1 GENIUSH

The vibrational and rovibrational eigenstates of VR and its deuterated isotopologues were computed with the in-house nuclear-motion code GENIUSH,[60–62] where GENIUSH stands for a general (GE), numerical (N) rovibrational program employing curvilinear internal (I) coordinates and user-specified (US) Hamiltonians (H). Within GENIUSH the wave function is represented on a full or reduced-dimensional grid by using the discrete variable representation (DVR) technique[63] and the resulting large-scale eigenvalue problem is solved iteratively by the Lanczos algorithm.[64] The latest version of the GENIUSH code utilizes the molecular symmetry (MS) group in the vibration-only mode of computation, yielding symmetry labels for the vibrational eigenstates in a natural way.[60] This feature of the GENIUSH code gains particular importance when the goal is the computation of a large number of vibrational eigenstates for a large(r) molecular system.

The rovibrational states computed with GENIUSH are labeled with the help of the rigid rotor decomposition (RRD) technique.[65] Within the RRD scheme the rovibrational eigenvectors are decomposed in the product basis of vibrational and rigid-rotor eigenstates, yielding the vibrational parents of the rovibrational state and the usual rotational quantum numbers.

The version of GENIUSH used during this study also allows computation of vibrational states in a contracted basis. This means that the full-dimensional problem is divided into two complementary reduced-dimensional subproblems and a selected number of their eigenstates is used to form a contracted direct-product basis for solving the full-dimensional problem. To illustrate this, suppose we select two groups of coordinates, $\mathbf{R}_A$ and $\mathbf{R}_B$. Subproblem A is described by the nuclear-motion Schrödinger equation

$$\hat{H}^{A}(\mathbf{R}_A;\mathbf{R}_B^{Ref})|A_m(\mathbf{R}_A;\mathbf{R}_B^{Ref})\rangle = E_m^{A}|A_m(\mathbf{R}_A;\mathbf{R}_B^{Ref})\rangle, \quad (1)$$

where $\mathbf{R}_B^{Ref}$ means a parametric dependence on the $\mathbf{R}_B$ coordinates in terms of a chosen reference geometry. Subproblem B is described in an analogous way,

$$\hat{H}^{B}(\mathbf{R}_B;\mathbf{R}_A^{Ref})|B_n(\mathbf{R}_B;\mathbf{R}_A^{Ref})\rangle = E_n^{B}|B_n(\mathbf{R}_B;\mathbf{R}_A^{Ref})\rangle. \quad (2)$$

Then the full-dimensional contracted basis function reads as

$$|\mathbf{R}_A\mathbf{R}_B\rangle_{mn} = |A_m(\mathbf{R}_A;\mathbf{R}_B^{Ref})\rangle \otimes |B_n(\mathbf{R}_B;\mathbf{R}_A^{Ref})\rangle, \quad (3)$$

where the desired number of eigenstates of the two subproblems is used in the contracted basis. Details concerning how the contracted code works within the GENIUSH scheme will be published in a separate paper.[66]

2.2 Potential energy surfaces (PES)

The present study utilizes two more or less global *ab initio* PESs available for VR.[36,39] The PES developed by Bowman *et al.*[36] is an 8th-order polynomial fit to 50 230 ROCCSD(T)/aug-cc-pVTZ energy points. The configuration space selected during the construction of this PES was meant to describe particularly well the dissociation channel $C_2H_3 \rightarrow C_2H_2 + H$. From here on, in this study this PES is called PES/D. The other PES described in the same paper of Bowman *et al.*,[36] referred to as PES/S and tailored to describe accurately the low-energy double well region, exhibited unphysical kinks when applied to our multi-dimensional models. Thus, PES/S was not considered further during the present study.

While this work was in progress, Yu *et al.*[40] published a rovibrational study of the ground electronic state of VR using their own PES.[39] Construction of this PES utilized 68 479 energy points computed at the UCCSD(T)-F12a/aug-cc-pVTZ level, describing well several isomerization reaction channels. The PES fit is based on neural networks and hence we refer to this PES in this work as the NN-PES. While using the NN-PES, we learned that the originally reported geometry parameters do not correspond to the true stationary points and energies, but they were somewhat shifted due to a grid representation used in the computations of ref. 67. In the present study the stationary point geometries were reoptimized for the use of

Table 4 Internal coordinate system (Coord.) used for the vinyl radical (see Fig. 2 for the notation) and parameters related to the discrete variable representation (DVR) basis sets employed during the variational vibrational computations. All the angular coordinates are treated internally as cosines. The starred Legendre bases are not scaled to match the given interval, the grid points spread naturally between −1 and +1. The number of grid points given in parentheses corresponds to the basis that was used for the rovibrational computations, where for technical reasons the basis size was reduced. The chosen reference geometry (ref. geom.) corresponds to the transition state of the $C_\alpha H$ rocking tunneling motion. The radial coordinates are given in bohr, the angular coordinates are given in degrees

		DVR points		PO-DVR points				Ref. geom.	
Coord.	DVR type	PES/D	NN-PES	PES/D	NN-PES	Min.	Max.	PES/D	NN-PES
R_{CC}	Hermite	300	300	9 (7)	8 (7)	2.1	3.1	2.47	2.46
R_1	Laguerre	300	300	6 (5)	6 (5)	1.3	3.4	2.06	2.06
R_2	Laguerre	300	300	6 (5)	6 (5)	1.3	3.4	2.06	2.06
R_3	Laguerre	300	300	6 (5)	6 (5)	1.3	3.4	2.02	2.01
ϑ_1	Legendre	300	300	10 (9)	12 (9)	1.0	89.0	32.3	32.2
ϑ_2	Legendre	300	300	10 (9)	12 (9)	1.0	89.0	32.3	32.2
ϑ_3	Legendre*	301	300 (301)	21 (21)	22 (21)	0.0	180.0	90.0	90.0
φ_1	Legendre*	301	300 (301)	13 (11)	12 (11)	0.0	180.0	90.0	90.0
φ_2	Legendre	301	301	13 (11)	13 (11)	3.0	177.0	90.0	90.0

the NN-PES. Another characteristic of the originally reported NN-PES is that it is not symmetric with respect to the exchange of the β hydrogens. We had to symmetrize the NN-PES for the present study by using the simple formula

$$E^{sym}(H_1, H_2) = \frac{1}{2}[E(H_1, H_2) + E(H_2, H_1)] \quad (4)$$

in order to obtain correct tunneling splittings.

Using two PESs of rather different origin and functional form helps ensure that the semiquantitative and qualitative findings of this variational nuclear-motion study are correct.

2.3 Coordinate system, basis sets, and masses

Fig. 2 shows the coordinate system chosen to describe the vibrations of the different isotopologues of VR. These coordinates are also convenient for studying the $C_\alpha H$ rocking tunneling motion. The parameters of the coordinates as well as the corresponding DVR parameters of the grid employed during the GENIUSH computations are listed in Table 4 for both the PES/D and NN-PES computations. Basis sets of different size were selected for use with the two PESs. What we call the large basis has been used in the vibration-only mode of computations and appropriately describes all 9 fundamental vibrations. The final form of a "smaller" basis correctly describes only six fundamental modes (all the bendings and the CC stretching) and their combinations and has been used in the rovibrational computations aimed at determining rotational shifts of the low-energy vibrations.

In addition, Table 4 contains the geometry parameters of the tunneling transition state structure, which serves as a reference structure in the reduced-dimensional and the potential optimized[68–70] discrete variable representation (PO-DVR) computations.

All the angular coordinates are internally treated as cosines of the angles. The DVR points of a given type are scaled to match the appropriate interval, except for the ϑ_3 and φ_1 coordinates, where the Legendre points naturally spread between −1 and +1 without any scaling.

The nuclear masses used in this study were m_H = 1.007276470 u, m_D = 2.014102000 u, and m_C = 12.0 u.

2.4 Harmonic frequencies

The computations of the quadratic force field and the related harmonic frequencies corresponding to the minimum and the $C_\alpha H$ rocking tunneling transition state were performed with the help of the CFOUR[71] program package.

The equilibrium structure and the quadratic force field were obtained at the same level to avoid the non-zero-force dilemma.[72] Results of an all-electron UCCSD(T)/aug-cc-pwCVQZ level harmonic vibrational analysis of VR are shown in Table 5 for CH_2═CH, CH_2═CD, CD_2═CD, and *syn*- and *anti*-CHD═CH, where *syn* and *anti* refer to the mutual position of the α and β hydrogens. The harmonic analysis utilized the INTDER package[72–74] and determined the total energy distributions (TED)[75,76] to characterize the normal modes corresponding to the equilibrium and transition state structures.

2.5 Focal-point analysis of the barrier height

The all-electron ROCCSD(T)/aug-cc-pCVQZ optimized geometries (the minimum and the transition state) served as reference structures for the FPA analysis of the tunneling barrier height. A series of computations employing the aug-cc-pCV*X*Z (*X* = 3, 4, 5, and 6) basis sets have been performed with both reference structures up to the CCSD(T) level of theory. Relativistic corrections were computed within the mass-velocity and one-electron Darwin (MVD1) approximation.[77,78] Diagonal Born–Oppenheimer corrections (DBOC)[79,80] were computed at the ROHF level of theory. All electronic-structure computations up to CCSD(T) were performed with the CFOUR[71] program package. Computations beyond CCSD(T) utilized the MRCC package.[81] The FPA results are summarized in Table 6.

Two complete basis set (CBS) extrapolation schemes were employed to improve our estimations for the energy difference between the two stationary structures. A three-parameter extrapolation formula of Peterson and co-workers,[82] denoted as CBS-A, and a 2-parameter scheme, denoted as CBS-B, which treated the HF level by the formula of Karton and Martin[83] and the correlated methods by the formula of Halkier *et al.*[84] were utilized.

Table 5 All-electron UCCSD(T)/aug-cc-pwCVQZ harmonic vibrational fundamentals, ω_i, in cm^{-1}, for $CH_2{=}CH$, $CH_2{=}CD$, $CD_2{=}CD$, and *syn*- and *anti*-$CHD{=}CH$ at the equilibrium structure of C_s point-group symmetry. The last column of the table provides the harmonic wavenumbers corresponding to the transition state structure (TS), with the C_{2v} point-group symmetry labels in parentheses for $CH_2{=}CH$

Molecule	i	Irrep.	ω_i	Assignment (total energy distribution)	TS
$CH_2{=}CH$	1	A′	3256.3	0.98 CH stretch	3432.6 (A_1)
	2	A′	3183.1	0.86 CH_2 asym. stretch	3094.2 (B_2)
	3	A′	3077.5	0.85 CH_2 sym. stretch	3040.3 (A_1)
	4	A′	1648.2	0.87 CC stretch	1646.0 (A_1)
	5	A′	1398.3	0.88 CH_2 bend	1421.5 (A_1)
	6	A′	1069.6	0.64 CH_2 rock − 0.37 CH rock	956.7 (B_2)
	7	A′	723.4	0.64 CH rock + 0.36 CH_2 rock	747.5i (B_2)
	8	A″	927.8	1.00 CH_2 oop wag	928.8 (B_1)
	9	A″	828.1	1.00 CH oop wag	680.3 (B_1)
$CH_2{=}CD$	1	A′	3183.1	0.86 CH_2 asym. stretch	3086.5
	2	A′	3078.5	0.86 CH_2 sym. stretch	3035.9
	3	A′	2424.3	0.93 CD stretch	2566.2
	4	A′	1613.4	0.78 CC stretch + 0.16 CH_2 bend	1576.5
	5	A′	1392.4	0.84 CH_2 bend − 0.15 CC stretch	1408.7
	6	A′	1020.5	0.82 CH_2 rock	949.5
	7	A′	580.9	0.82 CD rock	597.1i
	8	A″	917.6	1.00 CH_2 oop wag	912.7
	9	A″	687.8	1.00 CD oop wag	522.8
$CD_2{=}CD$	1	A′	2430.7	0.89 CD stretch	2568.4
	2	A′	2363.5	0.94 CD_2 asym. stretch	2294.3
	3	A′	2241.2	0.87 CD_2 sym. stretch	2204.8
	4	A′	1566.1	0.86 CC stretch	1535.0
	5	A′	1022.5	0.96 CD_2 bend	1031.2
	6	A′	872.8	0.62 CD_2 rock − 0.37 CD rock	738.2
	7	A′	523.0	0.62 CD rock + 0.38 CD_2 rock	592.9i
	8	A″	727.3	1.00 CD_2 oop wag	721.4
	9	A″	633.0	1.00 CD oop wag	521.3
$CHD{=}CH$ (*anti*/*syn*)	1	A′	3256.3/3255.8	0.98/0.99 $C_\alpha H$ stretch	3415.4
	2	A′	3095.7/3169.1	0.99/1.00 $C_\beta H$ stretch	3062.1
	3	A′	2332.6/2275.1	0.97/0.98 $C_\beta D$ stretch	2250.4
	4	A′	1623.1/1625.7	0.91/0.91 CC stretch	1613.1
	5	A′	1265.9/1271.9	0.80/0.82 $C_\beta HD$ bend	1279.4
	6	A′	969.5/989.0	0.53/0.58 $C_\beta HD$ rock − 0.34/0.35 $C_\alpha H$ rock	802.7
	7	A′	669.4/651.5	0.55/0.54 $C_\alpha H$ rock + 0.44/0.42 $C_\beta HD$ rock	763.2i
	8	A″	837.5/897.1	0.62/0.79 $C_\beta HD$ oop wag + 0.38/0.21 $C_\alpha H$ oop wag	831.1
	9	A″	788.2/761.9	0.62/0.79 $C_\alpha H$ oop wag − 0.38/0.21 $C_\beta HD$ oop wag	661.4

2.6 Wave function analysis

Assigning quantum labels to computed vibrational states is often based on wave-function plots and the node-counting technique. Using these approaches one attempts to identify the excited vibrational modes of a multidimensional wave function. While the node-counting method appears to be useful for small systems and low excitation energies, see, for example, ref. 85 and 86, it quickly becomes impractical and prone to errors for larger systems, when the number of vibrational degrees of freedom and the number of possible mode combinations increase.[87]

To at least partially remedy the situation, in this study one- and two-mode reduced density matrices, 1RDM and 2RDM, respectively, or rather only their diagonal elements,

$$\mathrm{D1RDM}(q_i) = \int \mathrm{d}q_1 \ldots \mathrm{d}q_{i-1}\mathrm{d}q_{i+1} \ldots \mathrm{d}q_N \; \Psi^*(q_1,\ldots,q_N)\Psi(q_1,\ldots,q_N) \tag{5}$$

and

$$\mathrm{D2RDM}(q_i,q_j) = \int \mathrm{d}q_1 \ldots \mathrm{d}q_{i-1}\mathrm{d}q_{i+1} \ldots \mathrm{d}q_{j-1}\mathrm{d}q_{j+1} \ldots \mathrm{d}q_N \; \Psi^*(q_1,\ldots,q_N)\Psi(q_1,\ldots,q_N), \tag{6}$$

are used for assigning the computed vibrational states.

D1RDM and D2RDM do not show a change in the sign of the wave function at a node, they only exhibit kinks in the mode density. The information provided by D1RDM and D2RDM is sufficient for the assignment of many computed wave functions as the density seemingly integrates out some of the misleading structural details characteristic of wave-function plots. The structure of the density plots depends only slightly on the particular grid employed and a much smaller number of density plots needs to be generated for assignment purposes as compared to the number of wave-function projections needed for node counting. Furthermore, density plots tend to be very regular even in multimodal excited states, helping semi-automatic assignment procedures. A particular advantage of D1RDM and

Table 6 Focal-point analysis of the barrier to linearity (in cm^{-1}) of the $C_\alpha H$ rocking motion of the vinyl radical[a]

	ΔE_e(HF)	δ[MP2]	δ[CCSD]	δ[CCSD(T)]	Δ[MVD1]	Δ[DBOC]
aug-cc-pCVTZ	2811.9	−1181.8	138.0	−45.9	2.5	5.1
aug-cc-pCVQZ	2821.3	−1203.3	161.2	−48.8	2.7	5.1
aug-cc-pCV5Z	2821.2	−1210.2	170.6	−49.3	2.7	**5.1**
aug-cc-pCV6Z	2821.2	−1215.4	174.9			
CBS-A(3,4,5)	[2821.1]	[−1214.3]	[176.2]	[−49.7]	[2.7]	
CBS-A(4,5,6)	[2821.2]	[−1218.4]	[177.4]			
CBS-B(4,5)	[2821.2]	[−1217.4]	[180.5]	[−**49.8**]	[**2.7**]	
CBS-B(5,6)	[**2821.2**]	[−**1222.5**]	[**180.8**]			

[a] The symbol δ denotes the increment in the relative energy (ΔE_e) with respect to the preceding level of theory in the hierarchy HF → MP2 → CCSD → CCSD(T). The diagonal Born–Oppenheimer correction (DBOC) values were computed at the ROHF level. Brackets signify results obtained from basis set extrapolations. The complete basis set (CBS) extrapolation schemes A and B are described in the text. The arguments of the CBS schemes are the cardinal numbers X of the basis sets involved in the extrapolation. Boldface entries represent the final values used to determine the barrier within the FPA scheme. The harmonic zero-point vibrational energy correction to the barrier height, ΔZPVE, is −99.5 and −94.6 cm^{-1} at the ROCCSD(T)/aug-cc-pCVQZ and UCCSD(T)/aug-cc-pwCVQZ levels, respectively. Their average, −97.0 cm^{-1} is our best estimate for ΔZPVE.

D2RDM for this study is that the (+) and (−) vibrational states are characterized by extremely similar plots (even more so than for the wave functions), helping considerably their pairing. A detailed report about the use of one- and two-mode reduced density matrices to assign vibrational states will be given elsewhere.[88]

3 Results and discussion

3.1 Contracted vibrational computations, a case study for CH_2═CH

The contracted computation scheme, see Section 2.1, has been thoroughly studied using only the PES/D potential. The most important results obtained helping to judge the performance of the different contraction schemes are shown in Table 7. The more limited results for the NN-PES potential are similar and thus are not given here.

The computationally most efficient contraction scheme is based on the five-dimensional bending and the four-dimensional stretching subspaces (5 + 4 scheme). Another scheme, in which the C═C stretching mode, which is relatively close in energy to the bending modes, was moved into the bending mode subspace (6 + 3 scheme), turned out to be computationally much more demanding; thus, we do not report results for the 6 + 3 scheme.

Table 7 shows absolute values of the differences between the uncontracted full-dimensional results and those obtained from various contracted computations. We show three sets of selected states (1–25: 0–1700 cm^{-1}, 51–75: 2260–2550 cm^{-1}, and 101–125: 2820–3020 cm^{-1}) to demonstrate that the error increases with increased excitation. Four different subspace sizes are presented in Table 7 using a fractional notation: the numerator denotes the size of the bending subspace, while the denominator shows the size of the stretching subspace used in the contracted 9D computations.

Table 7 Errors characterizing the vibration-only (J = 0) computations for the CH_2═CH radical, utilizing the PES/D potential, and employing different vibrational contraction schemes. The values are given in cm^{-1}. i is the state number, while the fractions represent different number of bending (*e.g.*, 205, 310, and 501) and stretching (*e.g.*, 26 and 40) states involved in the final, combined computation (see text for further details)

i	205/26	310/26	501/26	310/40	i	205/26	310/26	501/26	310/40	i	205/26	310/26	501/26	310/40
1	0.2	0.2	0.1	0.1	51	13.2	5.8	2.3	5.7	101	58.1	15.1	7.0	15.0
2	0.0	0.0	0.0	0.0	52	11.5	7.5	3.2	7.4	102	62.0	15.6	6.8	15.4
3	0.2	0.1	0.1	0.1	53	18.5	5.1	2.2	5.0	103	63.0	14.9	5.9	14.8
4	0.3	0.2	0.1	0.1	54	11.7	4.5	1.6	4.5	104	70.8	12.8	5.8	12.8
5	0.3	0.1	0.1	0.1	55	11.1	5.3	1.9	5.2	105	59.9	10.3	5.9	10.2
6	0.3	0.1	0.1	0.1	56	13.7	7.6	3.0	7.5	106	59.3	20.6	5.2	19.2
7	0.2	0.1	0.1	0.1	57	24.8	6.2	2.2	6.1	107	52.0	13.2	5.4	13.1
8	0.3	0.1	0.1	0.1	58	23.6	4.5	1.9	4.4	108	53.8	24.6	5.5	24.6
9	0.5	0.2	0.1	0.2	59	24.8	5.5	1.9	5.4	109	51.0	20.2	7.3	20.1
10	0.5	0.3	0.2	0.3	60	12.6	5.1	1.8	5.1	110	62.9	24.0	6.3	21.0
11	1.5	0.4	0.2	0.3	61	5.8	2.9	1.8	2.0	111	62.4	14.6	6.0	11.4
12	2.0	0.7	0.3	0.6	62	25.0	2.3	1.9	1.3	112	59.4	25.0	5.8	24.8
13	3.0	0.8	0.5	0.6	63	30.5	4.8	1.9	4.8	113	46.6	34.2	8.3	30.9
14	3.0	0.9	0.5	0.7	64	33.8	6.2	2.1	6.1	114	34.2	20.4	6.4	16.9
15	2.2	0.5	0.2	0.5	65	7.5	2.8	1.8	2.1	115	57.5	27.7	4.7	27.5
16	2.2	0.7	0.3	0.7	66	8.7	2.2	1.7	1.3	116	62.1	29.7	4.9	29.0
17	2.3	0.8	0.4	0.7	67	33.8	8.6	2.8	8.5	117	60.3	38.7	6.0	38.7
18	2.4	0.6	0.2	0.5	68	37.3	4.8	2.0	4.8	118	61.8	38.4	6.1	38.4
19	2.2	1.1	0.3	1.0	69	36.8	6.9	2.2	6.8	119	50.4	34.3	7.6	33.2
20	1.8	1.2	1.1	0.4	70	38.7	5.6	2.2	5.6	120	63.0	29.9	8.0	29.8
21	1.7	1.2	1.1	0.3	71	12.2	6.6	2.4	6.6	121	44.5	18.7	2.6	18.6
22	4.0	1.7	0.5	1.5	72	25.1	3.1	2.1	2.0	122	47.9	36.5	6.1	34.3
23	2.9	1.4	0.2	1.4	73	31.2	7.3	2.2	7.3	123	48.1	34.2	6.4	32.8
24	3.1	1.4	0.3	1.4	74	29.4	8.7	4.4	7.6	124	43.2	32.0	6.7	28.1
25	3.0	1.5	0.2	1.5	75	51.7	3.2	2.3	2.9	125	48.0	23.9	8.7	20.9

We can see that, as expected, the first 10 states are well described even by using the smallest subspaces. After that the error of the smallest subspace scheme exceeds 1 cm^{-1} and remains at this level for a few tens of other states. By increasing the number of states in the bending subspace from 205 to 310 we observe that the error decreases by about a factor of two. Further increase in the number of bending states, up to 501, causes the contraction error to practically disappear. Understandably, increasing the size of the stretching subspace did not have a considerable influence on the error, except for the states with a strong stretching character, like states #20 and #21, which are the $\nu_4^{\pm}$ (C═C stretch) fundamentals.

In the second set of states, *i.e.*, states 51–75, the errors characterizing the smallest contraction subspace results reach already several tens of cm^{-1}, while the larger subspace schemes successfully keep the error on the order of a few cm^{-1}.

For even higher-energy states, states 101–125, the error of the smallest subspace scheme is about 50 cm^{-1} and slowly rises further. From the larger subspace schemes only the 501/26 scheme provides values comparable to the uncontracted full-dimensional results, with the largest differences below 10 cm^{-1}. In the current implementation, however, the computational cost of the largest scheme is comparable to the uncontracted computation, as far as the CPU-time usage is considered.

Nevertheless, the contracted computation appears to be a viable option for computing a large number of vibrational states of larger systems.

As a rule of thumb, for a reliable contracted computation one has to balance the coordinate subspace dimensions and set the number of states in each of the subspaces so that they reach a few times higher energy than the energy of the highest state one is interested in. Note that the errors characterizing the largest, 501/26, computations are certainly smaller than, or comparable to, the error arising from the finite accuracy of the PES employed.

3.2 Structure and harmonic vibrational frequencies

The C_s point-group symmetry equilibrium structure of VR on its $\tilde{X}^2A'$ ground electronic state surface and the structure of the transition state hindering the $C_\alpha H$ rocking tunneling, of C_{2v} point-group symmetry, have been determined in this study at high levels of electronic structure theory (see Table 1). There is little doubt that the all-electron ROCCSD(T)/aug-cc-pCVQZ and UCCSD(T)/aug-cc-pwCVQZ structures obtained in this study represent very well, with uncertainties less than 0.003 Å and 0.5°, the ''true'' equilibrium structures of the minimum as well as of the TS. The ROCCSD(T)/aug-cc-pCVQZ structures served as the reference structures for the focal-point analysis of the $C_\alpha H$ rocking tunneling barrier height (see Table 6).

As clear from the comparison of data presented in Table 1, when the same level of theory is used for their determination, the global minimum (min) and the transition-state (TS) structures differ rather little. The most significant difference in the bond lengths is for R_3, the C_α–H distance, which drops from 1.077 (min) to 1.064 Å (TS). The shorter C_α–H bond length characterizing the TS structure indicates more efficient CH bonding due to the linear arrangement of the C═C–H fragment and a switch from sp^2 to sp hybridization on C_α (note that a qualitative picture based on hybridization arguments is given in Fig. 1 of ref. 35). It is also of interest to note that the equilibrium CH bond length in acetylene, C_2H_2, at 1.062 Å,[89] is just slightly shorter than that in the TS of CH_2═CH.

The equilibrium structural parameters determined for VR in this study can be compared with those available for vinyl derivatives: vinyl cyanide (acrylonitrile)[90,91] and vinyl acetylene (but-1-ene-3-yne).[92] The prototypical double bond length is 1.3305 Å in ethene,[93] similar to that found in vinyl cyanide and vinyl acetylene. The C═C bond length in VR, however, is considerably shorter, by about 0.02 Å, than in these two molecules. The C–H bond lengths of VR are similar to that of ethene, 1.0805(10) Å.[93] The shorter C_α–H bond length of VR compared to C_β–H is also in line with the increased bond strengths about C_α.

Due to the symmetry of VR, it is expected that the modes ν_1, ν_6, and ν_7 would couple most strongly during the in-plane rocking tunneling motion (this is mode ν_7). Consequently, these are the modes where the largest changes can be observed between the corresponding harmonic wavenumbers of the minimum and the TS (see Table 5).

It is worth discussing here a couple of harmonic vibrational analysis results relevant for the internal dynamics of VR (see Table 5). The very strong coupling at the harmonic level between the rocking internal coordinates characterizing the ν_6 and ν_7 modes of VR suggests that the tunneling motion, formally associated with ν_7, may be more complex than naively expected. The D substitution on C_α has basically no effect on the CH_2 stretching modes, suggesting an almost perfect decoupling of these A′-symmetry modes. There is much stronger coupling among the CC stretch and the bend modes, though the ''CH_2 bend'' is decoupled from the ''$C_\alpha H$ rock'' motion.

3.3 Tunneling barriers

There are two barriers one must investigate when H-atom tunneling in VR is considered. The barrier hindering the in-plane $C_\alpha H$ rocking tunneling motion has been investigated before both computationally[26,27] and experimentally.[11,15] The second barrier hinders the scrambling of the protons attached to C_α and C_β and it is characterized by a much longer tunneling path and a much larger barrier. As noted before, we deemed it sufficient to consider only the $C_\alpha H$ rocking tunneling barrier during this study, where an upper limit of about 3200 cm^{-1} is placed on the vibrational excitation.

The most relevant results of the FPA analysis of the barrier height hindering tunneling in VR are as follows (see Table 6): (a) as usual, the HF contribution converges very quickly, basically exponentially, to the CBS limit; (b) while the correlation contribution is substantial, most of it is recovered at the MP2 level, for which even the aug-cc-pCV6Z basis, close to the CBS limit, can be afforded; (c) different extrapolation schemes to the CBS limit yield results from which a relatively small uncertainty of 8 cm^{-1} can be attached to the MP2 CBS value, chosen to be obtained from the two largest basis set results (CBS-B(5,6)); (d) since double substitutions provide an increment of about −1000 cm^{-1}, triple substitutions of only −50 cm^{-1}, and the (Q) correction is just a few cm^{-1} (the CCSDT – CCSD(T) and the CCSDT(Q) – CCSDT increments, not reported in Table 6 as they have been computed using the UCC formalism, are about +10 and −4 cm^{-1}, respectively), it seems certain that further, even higher-order substitutions in the coupled-cluster series would not yield a correction larger than a couple of cm^{-1}, which can be considered as part of the uncertainty of the present final result; and (e) the overall uncertainty of the CBS CCSD(T) value is 15 cm^{-1}, which already includes the uncertainties of the relativistic and DBOC values as well as the missing higher-order coupled-cluster corrections. Thus, we estimate the $C_\alpha H$ rocking tunneling barrier of VR to be 1738(15) cm^{-1}. Inclusion of the ZPVE correction, −97(20) cm^{-1}, determined only within the harmonic oscillator approximation though at high levels of electronic structure theory, yields the ultimate tunneling barrier estimate of this study of 1641(25) cm^{-1}. Almost half of the uncertainty in the barrier height comes from the lack of consideration of anharmonicity in the ZPVE correction.

The 1641(25) cm^{-1} FPA estimate agrees well with some of the best previous estimates of the tunneling barrier. In particular, it is close to the best estimate provided by Tanaka *et al.*,[15] 1580(100) cm^{-1}. Our first-principles estimate also coincides

Table 8 Vibrational energy levels, obtained using the NN-PES,[40] of the vinyl radical, blocked by symmetry species of the C_{2v}(M) MS group. The present variational results are compared to those of Yu *et al.*[40] obtained utilizing the same NN-PES. The wavenumbers are given in cm^{-1}

i	$\tilde{\nu}(a_1)$	Yu[40]	Label	$\tilde{\nu}_i(a_2)$	Yu[40]	Label	$\tilde{\nu}(b_2)$	Yu[40]	Label	$\tilde{\nu}(b_1)$	Yu[40]	Label
1	0.0	0.0	GS^+	757.2	757.2	ν_9^-	0.6	0.5	GS^-	755.7	755.1	ν_9^+
2	665.9	667.5	ν_7^+	890.3	890.4	ν_8^-	679.6	681.4	ν_7^-	889.7	889.7	ν_8^+
3	991.4	996.3	ν_6^+	1433.4	1435.0	$(\nu_7+\nu_9)^-$	1005.1	1009.8	ν_6^-	1403.9	1405.0	$(\nu_7+\nu_9)^+$
4	1246.0	1247.5	$2\nu_7^+$	1573.1	1575.5	$(\nu_7+\nu_8)^-$	1350.5	1356.4	$2\nu_7^-$	1558.3	1560.4	$(\nu_7+\nu_8)^+$
5	1355.2	1357.8	ν_5^+	1758.2	1762.8	$(\nu_6+\nu_9)^-$	1357.8	1359.4	ν_5^-	1732.7	1737.5	$(\nu_6+\nu_9)^+$
6	1501.1	1500.9	$2\nu_9^+$	1896.0	1902.5	$(\nu_6+\nu_8)^-$	1504.7	1505.0	$2\nu_9^-$	1882.3	1888.9	$(\nu_6+\nu_8)^+$
7	1554.4	1569.2	$(\nu_6+\nu_7)^+$	2106.8	2113.5	$(2\nu_7+\nu_9)^-$	1582.8	1584.4	ν_4^-	1956.3	1957.0	$(2\nu_7+\nu_9)^+$
8	1583.3	1583.6	ν_4^+	2112.6	2115.5	$(\nu_5+\nu_9)^-$	1640.6	1659.2	$(\nu_6+\nu_7)^-$	2110.5	2112.3	$(\nu_5+\nu_9)^+$
9	1647.4	1646.8	$(\nu_8+\nu_9)^+$	2237.3	2243.3	$(\nu_5+\nu_8)^-$	1651.4	1647.8	$(\nu_8+\nu_9)^-$	2139.1	2141.5	$(2\nu_7+\nu_8)^+$
10	1780.8	1781.2	$2\nu_8^+$	2240.7	2241.6	$3\nu_9^-$	1782.1	1782.5	$2\nu_8^-$	2235.5	2236.0	$3\nu_9^+$
11	1841.8	1851.3	$3\nu_7^+$	2252.3	2256.8	$(2\nu_7+\nu_8)^-$	1948.1	1968.6	$(\nu_6,\nu_7)^-$	2239.2	2243.4	$(\nu_5+\nu_8)^+$
12	1992.4	2012.4	$2\nu_6^+$	2331.7	2333.9	$(\nu_4+\nu_9)^-$	2024.0	2043.5	$(\nu_5+\nu_7)^-$	2305.6	2320.6	$(\nu_6+\nu_7+\nu_9)^+$
13	2016.4	2027.0	$(\nu_5+\nu_7)^+$	2396.9	2412.1	$(\nu_6+\nu_7+\nu_9)^-$	2034.3	2039.8	$(\nu_6,\nu_7)^-$	2331.4	2331.3	$(\nu_4+\nu_9)^+$
14	2125.2	2127.1	$(\nu_7+2\nu_9)^+$	2401.4	2399.7	$(\nu_8+2\nu_9)^-$	2179.2	2182.7	$(\nu_7+2\nu_9)^-$	2395.6	2396.1	$(\nu_8+2\nu_9)^+$
15	2192.2	2220.3	$(\nu_6+2\nu_7)^+$	2464.8	2466.5	$(\nu_4+\nu_8)^-$	2254.4	2260.9	$(\nu_4+\nu_7)^-$	2447.1	2467.4	$(\nu_6+\nu_7+\nu_8)^+$
16	2244.7	2249.8	$(\nu_4+\nu_7)^+$	2531.3	2556.4	$(\nu_6+\nu_7+\nu_8)^-$	2315.6	2328.5	$(\nu_6,\nu_7)^-$	2466.0	2466.0	$(\nu_4+\nu_8)^+$
17	2297.5	2299.9	$(\nu_7+\nu_8+\nu_9)^+$	2546.0	2541.2	$(2\nu_8+\nu_9)^-$	2330.8	2340.6	$(\nu_7+\nu_8+\nu_9)^-$	2540.0	2540.4	$(2\nu_8+\nu_9)^+$
18	2327.7	2351.6	$(\nu_5+\nu_6)^+$	2667.1	2689.7	$(3\nu_7+\nu_9)^-$	2344.7	2364.6	$(\nu_5+\nu_6)^-$	2599.1	2608.8	$(3\nu_7+\nu_9)^+$
19	2447.9	2453.8	$(\nu_7+2\nu_8)^+$	2675.9	2676.8	$3\nu_8^-$	2415.3	2455.5	$(\nu_6+3\nu_7)^-$	2673.0	2674.6	$3\nu_8^+$
20	2459.8	2467.2	$(\nu_6+2\nu_9)^+$	2780.7	2762.9	$(\nu_5+\nu_7+\nu_9)^-$	2469.4	2477.1	$(\nu_7+2\nu_8)^-$	2735.5	2749.8	$(3\nu_7+\nu_8)^+$
21	2511.7	2709.6	$4\nu_7^+$	2792.2	2767.1	$(2\nu_6+\nu_9)^-$	2505.6	2513.2	$(\nu_6+2\nu_9)^-$	2745.5	2767.1	$(2\nu_6+\nu_9)^+$
22	2563.9	2584.2	$(\nu_4+\nu_6)^+$	2840.9	2749.8	$(3\nu_7+\nu_8)^-$	2576.7	2556.6	$(\nu_4+\nu_6)^-$	2754.0	2762.9	$(\nu_5+\nu_7+\nu_9)^+$
23	2599.4	2611.4	$(\nu_5+2\nu_7)^+$	2911.1	2930.7	$(\nu_5+\nu_7+\nu_8)^-$	2650.5	2658.9	$(\nu_6+\nu_8+\nu_9)^-$	2834.3	2836.7	$(\nu_7+3\nu_9)^+$
24	2625.2	2634.1	$(\nu_6+\nu_8+\nu_9)^+$	2920.0	2943.9	$(\nu_7+3\nu_9)^-$	2685.0	2717.9	$(\nu_5+2\nu_7)^-$	2883.3	2910.6	$(2\nu_6+\nu_8)^+$
25	2634.8	2866.3	$(2\nu_7+2\nu_9)^+$	2929.6	2916.5	$(2\nu_6+\nu_8)^-$	2701.9	2710.2	$2\nu_5^-$	2901.5	2923.9	$(\nu_5+\nu_7+\nu_8)^+$
26	2695.4	2570.8	$(2\nu_6+\nu_7)^+$	3000.7	2992.4	$(\nu_4+\nu_7+\nu_9)^-$	2709.0	2652.5	$(\nu_6,\nu_7)^-$	2958.1	3006.7	$(\nu_6+2\nu_7+\nu_9)^+$
27	2696.9	2710.4	$2\nu_5^+$	3076.2	3081.5	$(\nu_7+\nu_8+2\nu_9)^-$	2788.2	2799.0	$(\nu_6+2\nu_8)^-$	2975.3	2977.6	$(\nu_4+\nu_7+\nu_9)^+$
28	2773.9	2784.8	$(\nu_6+2\nu_8)^+$	3088.1	3123.8	$(\nu_5+\nu_6+\nu_9)^-$	2846.5	2747.3	$(2\nu_7+2\nu_9)^-$	3022.3	3025.8	$(\nu_7+\nu_8+2\nu_9)^+$
29	2819.1	2828.5	$(\nu_4+2\nu_7)^+$	3099.2	3093.6	$(\nu_6+2\nu_7+\nu_9)^-$	2857.6	2861.7	$(\nu_5+2\nu_9)^-$	3067.9	3103.4	$(\nu_5+\nu_6+\nu_9)^+$
30	2845.0	2855.7	$(\nu_6+3\nu_7)^+$	3137.3	3148.2	$(\nu_4+\nu_7+\nu_8)^-$	2891.4	2966.8	$(\nu_6,\nu_7)^-$	3088.1	3118.4	$(\nu_6+2\nu_7+\nu_8)^+$
31	2851.7	3076.6	$(2\nu_7+\nu_8+\nu_9)^+$	3152.3		$(2\nu_6+\nu_7+\nu_9)^-$	2898.9	2903.9	ν_3^-	3129.3	3136.7	$(\nu_4+\nu_7+\nu_8)^+$
32	2857.0	2859.6	$(\nu_5+2\nu_9)^+$	3208.2		$(\nu_6+2\nu_7+\nu_8)^-$	2917.9	2899.8	$(\nu_4+2\nu_7)^-$	3174.9	3197.7	$(\nu_6+3\nu_9)^+$
33	2879.4	2926.5	$(\nu_5+\nu_6+\nu_7)^+$	3224.0		$(\nu_7+2\nu_8+\nu_9)^-$	2941.9	2947.9	$(\nu_4+\nu_5)^-$	3194.1	3200.5	$(\nu_7+2\nu_8+\nu_9)^+$
34	2900.3	2903.7	ν_3^+	3234.7		$(2\nu_6+\nu_7+\nu_8)^-$	2962.8	2969.9	$4\nu_9^-$	3208.3		$(\nu_5+\nu_6+\nu_8)^+$
35	2912.1	2976.8	$3\nu_6^+$	3245.3		$(\nu_6+3\nu_9)^-$	2964.0	3012.9	$(\nu_5+\nu_6+\nu_7)^-$			
36	2941.8	2946.8	$(\nu_4+\nu_5)^+$				2996.3	3002.5	$(\nu_5+\nu_8+\nu_9)^-$			
37	2956.4	2960.0	$4\nu_9^+$				3002.5	2928.8	$(2\nu_7+\nu_8+\nu_9)^-$			
38	2995.6	3001.6	$(\nu_5+\nu_8+\nu_9)^+$				3018.2	3022.9	ν_2^-			
39	3018.5	3022.5	ν_2^+				3042.8	3016.5	$(\nu_6,\nu_7)^-$			
40	3034.5		$(2\nu_7+2\nu_8)^+$				3072.0	3074.8	$(\nu_4+2\nu_9)^-$			
41	3052.4		$(\nu_6+\nu_7+2\nu_9)^+$				3098.6		$(\nu_6,\nu_7)^-$			
42	3069.8	3069.9	$(\nu_4+2\nu_9)^+$				3121.7	3121.1	ν_1^-			
43	3115.8	3142.2	$(\nu_4+\nu_6+\nu_7)^+$				3122.6	3131.4	$(\nu_5+2\nu_8)^-$			
44	3121.1	3120.5	ν_1^+				3136.3	3127.2	$(\nu_8+3\nu_9)^-$			
45	3122.6	3132.9	$(\nu_5+2\nu_8)^+$				3151.7	3142.8	$(2\nu_7+2\nu_8)^-$			
46	3133.4	3106.6	$(\nu_8+3\nu_9)^+$				3156.0	3160.9	$2\nu_4^-$			
47	3159.1	3159.9	$2\nu_4^+$									

with a carefully obtained empirical estimate of Nesbitt and Dong,[35] 1602(20) cm^{-1}.

3.4 Vibrational states of $CH_2{=}CH$

The variational results obtained using the PES/D potential[36] exhibit a ν_9 fundamental at 835 cm^{-1}, higher than the corresponding harmonic value, 799 cm^{-1}. This unusual result turned out to be due to an insufficient description of the out-of-plane $C_\alpha H$ wagging motion obtained in the PES/D fit. This problem leads to overestimation of the ν_9 fundamental in all the deuterated VR computations, as well. We thus present only the results obtained with the NN-PES potential in this and the remaining sections discussing rovibrational states of VR and its deuterated isotopologues.

The computed vibrational (J = 0, where J stands for the quantum number describing the overall rotation of the molecule) states including all the fundamental modes are shown in Table 8. The computed states are labeled according to the irreducible representations of the C_{2v}(M) molecular symmetry (MS) group[55] and vibrational assignments are also provided in Table 8.

The assignments given in Table 8 are based principally on plots of the diagonal elements of the one- and two-mode reduced density matrices, D1RDM and D2RDM, respectively, introduced in eqn (5) and (6). As examples of highly descriptive

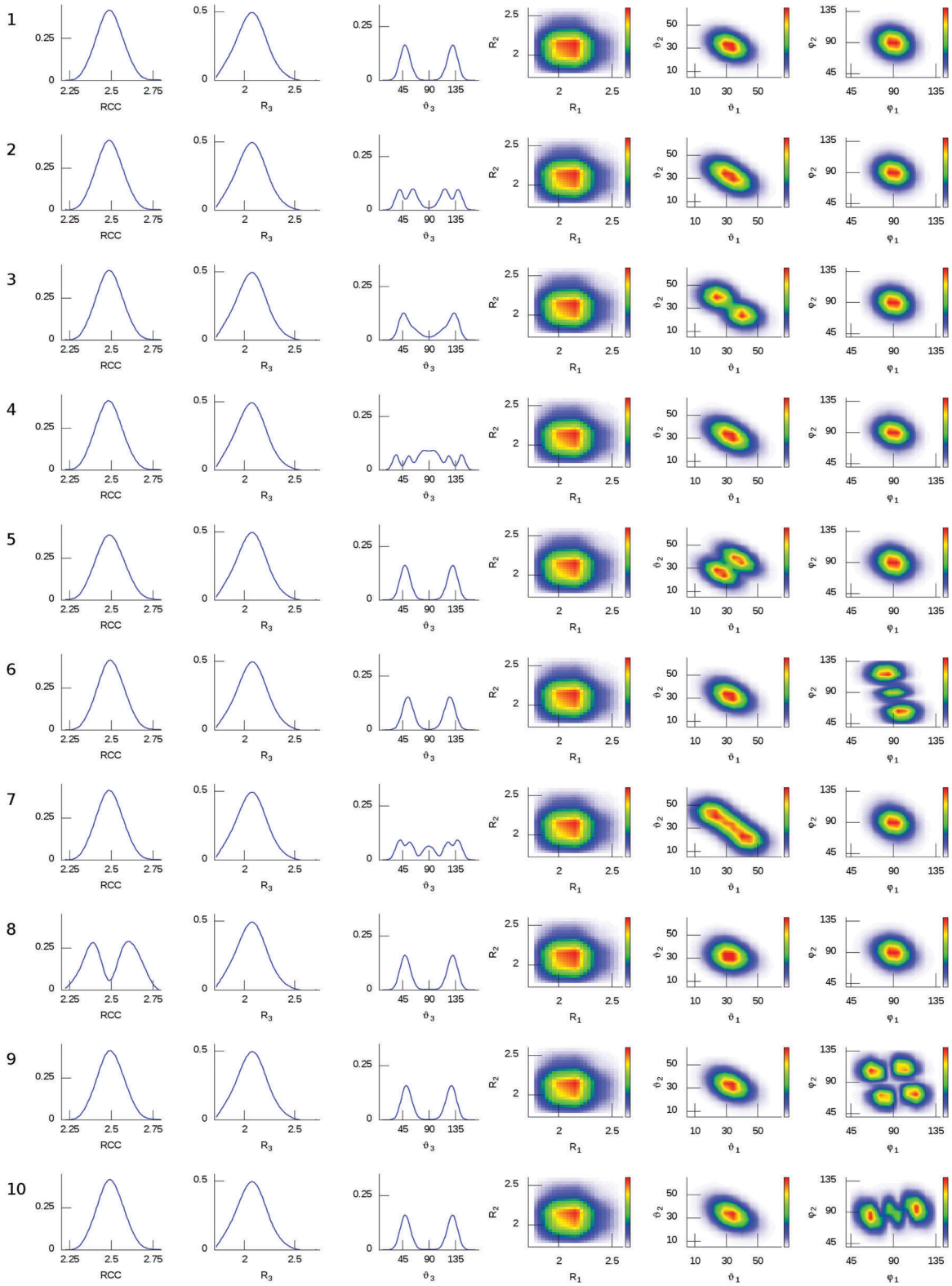

Fig. 3 D1RDM and D2RDM plots of the first 10 vibrational states of A_1 symmetry of CH_2═CH, showing clearly the utility of these plots to assign quantum numbers to the computed vibrational states. Radial coordinates are in bohr, angular coordinates are in degrees.

density plots, the first 10 vibrational states of VR of A_1 symmetry are shown in Fig. 3. Fig. 4 shows ambiguous states of the same A_1 symmetry block, whereby assigning quantum numbers to the computed states proved to be problematic if not impossible. The density plots of Fig. 3 and 4 involve the 9 vibrational modes as three 1D and three 2D plots. The 2D plots involve

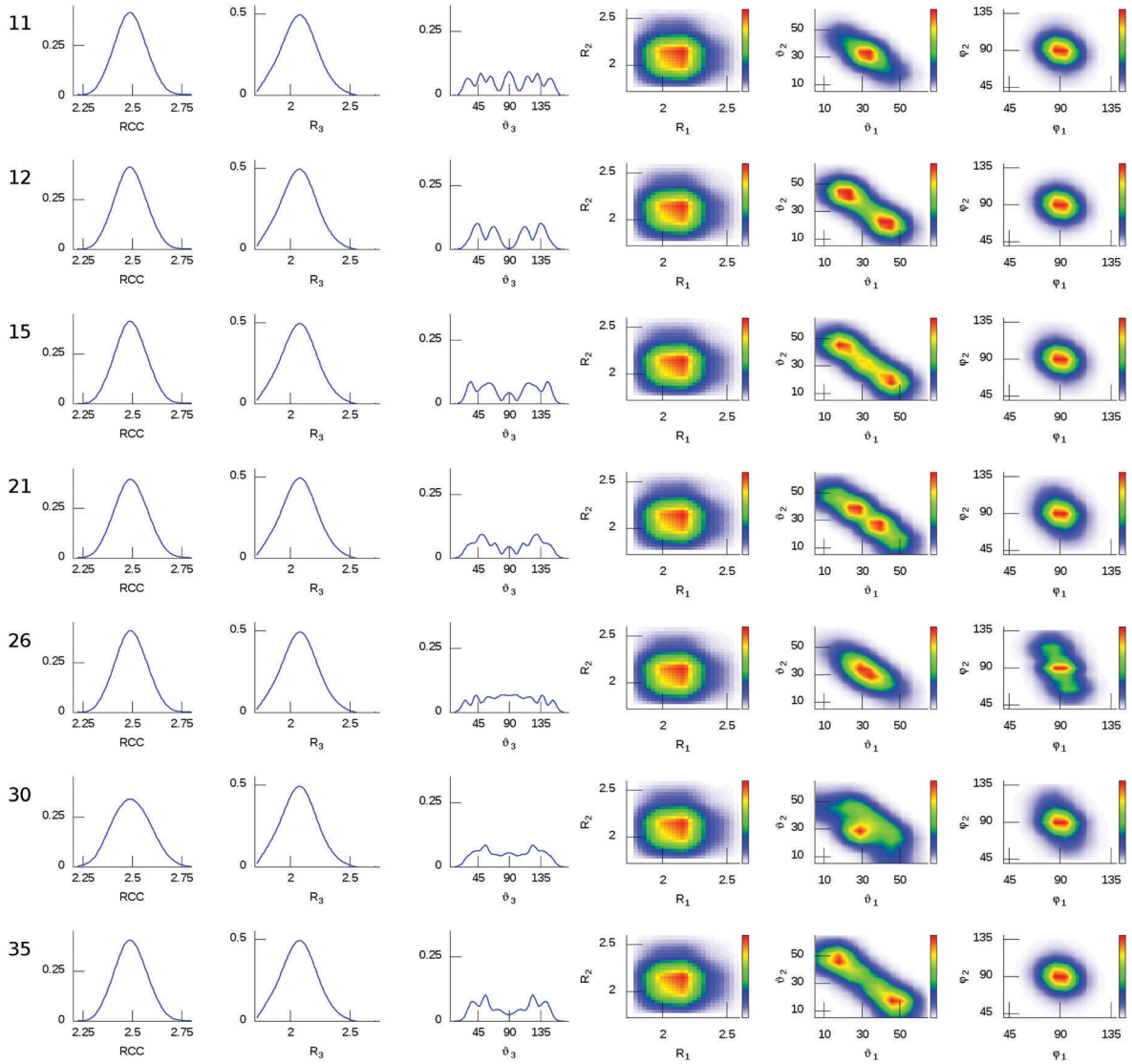

Fig. 4 D1RDM and D2RDM plots of selected vibrational states of $CH_2{=}CH$ of A_1 symmetry beyond state #10 and multiply excited along ν_6 and ν_7. Radial coordinates are in bohr, angular coordinates are in degrees.

related curvilinear coordinates, like ϑ_1 and ϑ_2, which form the CH_2 bending, ν_5, and CH_2 rocking, ν_6, modes.

As Fig. 3 shows, assigning quantum states based on D1RDM and D2RDM plots was successful for states below the $C_\alpha H$ rocking tunneling barrier. We can immediately observe in Fig. 3 the symmetric density distribution along the ϑ_3 coordinate of the ground vibrational state (state #1), confirming the effective C_{2v}(M) symmetry of the internal dynamics of VR. At places where the wave function has a node, the density exhibits a kink, as can clearly be seen for ν_7 (state #2) and ν_4 (state #8). $2\nu_9$ (state #6), $(\nu_8 + \nu_9)$ (state #9), and $2\nu_8$ (state #10) combinations are also clearly recognizable *via* the D2RDM plots. ν_5 (state #5) and ν_6 (state #3) excitations are distinguished as a positive or negative combination of the appropriate coordinates. The plots of the (−) states of B_2 symmetry are very similar to their (+) counterparts of A_1 symmetry, and an analogous statement holds for the B_1 and A_2 state pairs.

For states higher than the 10th in each symmetry block that involve multiple ν_6 or ν_7 excitations, the correct assignment becomes extremely difficult and our attempts resulted in contradictions. During the harmonic analysis (Table 5) we have observed that the two rocking motions contributing to the ν_6 and ν_7 modes of VR are strongly coupled. In the density plots we can see very strong interaction of the two modes. If density plots and simple energy decomposition rules[85] are applied to multiply excited states involving the ν_6 and ν_7 modes, they lead to controversies. Thus, labeling of such A_1-symmetry states corresponds to simple energy ordering, while the corresponding strongly-mixed B_2-symmetry states are labeled as $(\nu_6,\nu_7)^-$.

Table 8 also allows us to compare the present assignments with those of Yu *et al.*[40] Clearly, the state ordering is mostly the same with a few remarkable exceptions, like the case of the $4\nu_7^+$, $(2\nu_7 + 2\nu_9)^+$, and $(2\nu_7 + \nu_8 + \nu_9)^+$ states, which are shifted up by about 200 cm^{-1}.

Table 9 Vibrational energy levels, $\tilde{\nu}_i^+$, and tunneling splittings, $\tilde{\nu}_i^- - \tilde{\nu}_i^+$, of the fundamentals of the vinyl radical and its CH_2═CD and CD_2═CD deuterated isotopologues, as computed by GENIUSH on the NN-PES potential. For comparison, the results of Yu *et al.*[40] for the parent isotopologue are also provided. The wavenumbers are given in cm^{-1}

	CH_2═CH	CH_2═CH[40]	CH_2═CD	CD_2═CD
$\tilde{\nu}_1^+$	3121.12	3120.46		
$\Delta\tilde{\nu}_1$	0.56	0.68		
$\tilde{\nu}_2^+$	3018.49	3022.53		
$\Delta\tilde{\nu}_2$	−0.25	0.36		
$\tilde{\nu}_3^+$	2900.26	2903.70		
$\Delta\tilde{\nu}_3$	−1.33	0.19		
$\tilde{\nu}_4^+$	1583.26	1583.59	1558.85	1508.38
$\Delta\tilde{\nu}_4$	−0.51	0.76	−6.67	0.34
$\tilde{\nu}_5^+$	1355.24	1357.82	1350.03	1000.80
$\Delta\tilde{\nu}_5$	2.59	1.59	0.08	0.43
$\tilde{\nu}_6^+$	991.43	996.27	963.97	830.54
$\Delta\tilde{\nu}_6$	13.69	13.55	4.40	1.61
$\tilde{\nu}_7^+$	665.89	667.48	543.93	497.07
$\Delta\tilde{\nu}_7$	13.68	13.91	1.72	0.89
$\tilde{\nu}_8^+$	889.70	889.72	880.48	698.72
$\Delta\tilde{\nu}_8$	0.64	0.65	0.04	0.02
$\tilde{\nu}_9^+$	755.66	755.14	629.89	582.96
$\Delta\tilde{\nu}_9$	1.51	2.08	0.15	0.07
ΔGS	0.59	0.53	0.04	0.03

For a clear comparison with the results of Yu *et al.*[40] and also with the deuterated isotopologues, Table 9 summarizes the computed fundamentals together with their predicted tunneling splittings. The results of the two variational studies are very close, with differences in either of the quantities between a fraction of a cm^{-1} and a few cm^{-1} at most. Douberly *et al.*,[23] when they discussed the ν_1 band, noted that the change in the tunneling splitting, going from GS to ν_1, is less than 0.03 cm^{-1} but they could not determine the sign. The difference predicted in this study is −0.03 cm^{-1}, rather different from the value of +0.15 cm^{-1} determined by Yu *et al.*[40] The stretching modes ν_2, ν_3, and ν_4 exhibit tunneling splittings of opposite sign in our study as compared to the work of Yu *et al.*[40] Although both studies use the same NN-PES potential, there are a few factors that can explain the differences. First, in our study we use the symmetrized variant of the NN-PES, see eqn (4). Second, the effect of using different sets of coordinates and different grid bases is negligible only if the results are converged with respect to the grid basis size. In their study Yu *et al.*[40] utilized a limited contracted scheme employing 500 diabatic states of the angular coordinate subspace, while true full-dimensional computations have been performed during the present study.

As to experiments and other theoretical studies (see Table 2), most of our computed fundamentals agree well with some of the spectroscopic data, especially those measured in He nanodroplets[23] or in noble gas matrices,[16] with differences on the order of a few cm^{-1}. In these cases the small differences between experiment and theory are clearly due to the limited accuracy of the NN-PES used.

The tunneling splittings computed for the vibrational states of CH_2═CH show interesting features worth discussing. If a mode is uncoupled from the two tunneling modes, as is the case for the $n\nu_8$ and $n\nu_9$ modes, the vibrational states and the splittings come in a very regular fashion. For example, the $n\nu_8^+$ states are at 889.7, 1780.8, and 2673.0 cm^{-1}, for n = 1, 2, 3, respectively, and the associated splittings are +0.6, +1.3, and +2.9 cm^{-1}, in order. The situation is very similar for the ν_9 modes, there the $n\nu_9$ states for n = 1, 2, 3 and 4 are 755.7, 1501.1, 2235.5, and 2956.4 cm^{-1}, respectively, while the associated splittings are +1.5, +3.6, +5.2, and +6.4 cm^{-1}, in order. Thus, both the vibrational progressions and the splittings behave very regularly. Further regularities can clearly be observed for other progressions not involving modes ν_6 and ν_7 by examining the data of Table 8.

3.5 Rovibrational states of CH_2═CH

Table 10 shows 72 computed rotational energy shifts for J = 1, corresponding to the lowest 24 vibrational states. The rovibrational assignment, *i.e.*, assigning the rovibrational states to their vibrational parents, was done with the help of rigid rotor decomposition (RRD) analysis.[65] All the studied rovibrational states could be assigned to a single dominant vibrational parent, mostly with RRD coefficients larger than 0.99, but at least 0.95.

The most relevant result of these computations is that CH_2═CH exhibits mainly rigid-rotor-type behavior; the variation in the computed 1_{01} shifts is particularly small across the

Table 10 Rotational energy level shifts, in cm^{-1}, of the lowest 24 vibrational states of the CH_2═CH radical for J = 1. Rotational shifts corresponding to the rigid-rotor model are shown in the last row

Vibrational parent	1_{01}	1_{11}	1_{10}
GS^+	2.02	8.85	8.99
GS^-	2.02	8.85	8.98
ν_7^+	2.00	8.19	8.30
ν_7^-	2.00	8.00	8.11
ν_9^+	2.04	9.41	9.55
ν_9^-	2.04	9.34	9.48
ν_8^+	2.02	8.76	8.88
ν_8^-	2.02	8.72	8.84
ν_6^+	2.02	9.73	9.86
ν_6^-	2.02	9.55	9.69
$2\nu_7^+$	2.00	8.41	8.52
$2\nu_7^-$	2.00	7.81	7.93
ν_5^+	2.05	8.90	9.04
ν_5^-	2.02	8.59	8.72
$(\nu_7 + \nu_9)^+$	1.98	8.16	8.24
$(\nu_7 + \nu_9)^-$	2.00	7.43	7.51
$2\nu_9^+$	2.05	10.45	10.58
$2\nu_9^-$	2.04	10.24	10.40
$(\nu_6 + \nu_7)^+$	2.01	7.24	7.34
$(\nu_7 + \nu_8)^+$	2.01	8.00	8.10
$(\nu_7 + \nu_8)^-$	2.00	9.52	9.59
ν_4^+	2.03	8.94	9.08
ν_4^-	2.01	8.92	9.05
$(\nu_6 + \nu_7)^-$	2.01	8.88	9.00
Rigid rotor	2.03	8.73	8.87

vibrational states studied. The rovibrational interaction results in energy levels which almost mimic the rotation of a symmetric top; the rigid-rotor 1_{10}–1_{11} difference of 0.14 cm^{-1} decreases to 0.07 cm^{-1} for $(\nu_7 + \nu_8)^-$.

3.6 Vibrational energies and wave functions of CH_2═CD and CD_2═CD

Almost 50 vibrational (J = 0) states covering all 5 bending and the C═C stretching modes of the CH_2═CD and CD_2═CD isotopologues are shown, together with their C_{2v}(M) symmetry labels and assignments, in Tables 11 and 12, respectively.

As expected, all the vibrational states involving motion of a D atom have significantly lower energies. For CH_2═CD, the largest changes concern $\nu_7^{\pm}$ and $\nu_9^{\pm}$, in complete agreement with the harmonic vibrational analysis results (Table 5). For the fully deuterated CD_2═CD isotopologue, again as expected (Table 5), only the C═C stretching fundamental, $\nu_4^{\pm}$, is left more or less unchanged by perdeuteration. Attaching quantum numbers to the computed vibrational states *via* the D1RDM and D2RDM plots proved to be straightforward. In Table 9 we can see how the energies of the fundamentals are reduced systematically from the parent CH_2═CH to CH_2═CD and CD_2═CD.

As to the splittings, they are reduced by an order of magnitude with respect to the parent VR due to the isotopic effect (see Table 9). For the ground state the computed values match very well the experimental values of Tanaka *et al.*[20,24] (see also Table 3). Almost all of the tunneling splittings of the higher states show a regular pattern. One exception concerns the $\nu_5^{\pm}$ bending mode, whereby the fully deuterated isotopologue exhibits a larger splitting than the singly deuterated one. Another interesting case is the $\nu_4^{\pm}$ C═C stretching mode, where in the CH_2═CD species the negative splitting is enlarged by more than 6 cm^{-1} compared to the parent VR, and then shrinks to a positive value of +0.34 cm^{-1} in the fully deuterated case.

There are only a few experimental results available for the deuterated isotopologues (see Table 3), but all our predicted fundamental frequencies are in good agreement with the available measured spectroscopic data.

3.7 Vibrational states of CHD═CH

Even though the electronic PES used to study the rovibrational dynamics of CHD═CH is the same as that employed for CH_2═CH, CH_2═CD, and CD_2═CD, asymmetric deuteration on C_β, due to zero-point energy effects, results in an asymmetric

Table 11 Vibrational (J = 0) states of the CH_2═CD radical. The states are labeled by irreducible representations of the C_{2v}(M) molecular symmetry group and appropriate assignments are also given (see text for details). The wavenumbers are in cm^{-1}

i	$\tilde{\nu}_i(a_1)$	Label	$\tilde{\nu}_i(a_2)$	Label	$\tilde{\nu}_i(b_2)$	Label	$\tilde{\nu}_i(b_1)$	Label
1	0.00	GS^+	630.04	ν_9^-	0.04	GS^-	629.89	ν_9^+
2	543.93	ν_7^+	880.52	ν_8^-	545.65	ν_7^-	880.48	ν_8^+
3	963.97	ν_6^+	1171.32	$(\nu_7 + \nu_9)^-$	968.37	ν_6^-	1166.42	$(\nu_7 + \nu_9)^+$
4	1052.11	$2\nu_7^+$	1427.64	$(\nu_7 + \nu_8)^-$	1075.89	$2\nu_7^-$	1425.91	$(\nu_7 + \nu_8)^+$
5	1251.10	$2\nu_9^+$	1595.04	$(\nu_6 + \nu_9)^-$	1251.57	$2\nu_9^-$	1580.49	$(\nu_6 + \nu_9)^+$
6	1350.03	ν_5^+	1697.13	$(2\nu_7 + \nu_9)^-$	1350.11	ν_5^-	1651.37	$(2\nu_7 + \nu_9)^+$
7	1387.83	$(\nu_6 + \nu_7)^+$	1851.53	$(\nu_6 + \nu_8)^-$	1473.85	$(\nu_6 + \nu_7)^-$	1847.06	$(\nu_6 + \nu_8)^+$
8	1512.40	$(\nu_8 + \nu_9)^+$	1864.38	$3\nu_9^-$	1512.58	$(\nu_8 + \nu_9)^-$	1862.92	$3\nu_9^+$
9	1534.77	$3\nu_7^+$	1959.32	$(2\nu_7 + \nu_8)^-$	1552.18	ν_4^-	1934.90	$(2\nu_7 + \nu_8)^+$
10	1558.85	ν_4^+	1981.69	$(\nu_5 + \nu_9)^-$	1608.07	$3\nu_7^-$	1975.39	$(\nu_6 + \nu_7 + \nu_9)^+$
11	1763.59	$2\nu_8^+$			1763.63	$2\nu_8^-$		
12	1776.35	$(\nu_7 + 2\nu_9)^+$			1788.83	$(\nu_7 + 2\nu_9)^-$		
13	1814.35	$(\nu_6 + 2\nu_7)^+$			1893.04	$(\nu_5 + \nu_7)^-$		
14	1892.34	$(\nu_5 + \nu_7)^+$			1901.12	$2\nu_6^-$		

Table 12 Vibrational (J = 0) states of the CD_2═CD radical computed by GENIUSH. The states are labeled by irreducible representations of the C_{2v}(M) molecular symmetry group and an assignment based on harmonic modes is also given. The wavenumbers are in cm^{-1}

i	$\tilde{\nu}_i(a_1)$	Label	$\tilde{\nu}_i(a_2)$	Label	$\tilde{\nu}_i(b_2)$	Label	$\tilde{\nu}_i(b_1)$	Label
1	0.00	GS^+	583.03	ν_9^-	0.03	GS^-	582.96	ν_9^+
2	497.07	ν_7^+	698.74	ν_8^-	497.96	ν_7^-	698.72	ν_8^+
3	830.54	ν_6^+	1079.97	$(\nu_7 + \nu_9)^-$	832.15	ν_6^-	1077.98	$(\nu_7 + \nu_9)^+$
4	977.48	$2\nu_7^+$	1197.88	$(\nu_7 + \nu_8)^-$	988.54	$2\nu_7^-$	1197.01	$(\nu_7 + \nu_8)^+$
5	1000.80	ν_5^+	1410.65	$(\nu_6 + \nu_9)^-$	1001.23	ν_5^-	1407.15	$(\nu_6 + \nu_9)^+$
6	1158.56	$2\nu_9^+$	1533.01	$(\nu_6 + \nu_8)^-$	1158.77	$2\nu_9^-$	1531.23	$(\nu_6 + \nu_8)^+$
7	1262.08	$(\nu_6 + \nu_7)^+$	1568.87	$(2\nu_7 + \nu_9)^-$	1284.42	$(\nu_8 + \nu_9)^-$	1547.05	$(2\nu_7 + \nu_9)^+$
8	1284.52	$(\nu_8 + \nu_9)^+$	1584.98	$(\nu_5 + \nu_9)^-$	1297.06	$(\nu_6 + \nu_7)^-$	1584.49	$(\nu_5 + \nu_9)^+$
9	1396.54	$2\nu_8^+$	1688.74	$(2\nu_7 + \nu_8)^-$	1396.84	$2\nu_8^-$	1678.26	$(2\nu_7 + \nu_8)^+$
10	1421.40	$3\nu_7^+$	1698.84	$(\nu_5 + \nu_8)^-$	1477.67	$3\nu_7^-$	1697.92	$(\nu_5 + \nu_8)^+$
11	1496.17	$(\nu_5 + \nu_7)^+$			1497.55	$(\nu_5 + \nu_7)^-$		
12	1508.38	ν_4^+			1508.72	ν_4^-		
13	1614.46	$2\nu_6^+$			1643.90	$2\nu_6^-$		
14	1651.25	$(\nu_7 + 2\nu_9)^+$			1657.04	$(\nu_7 + 2\nu_9)^-$		

Table 13 Vibrational (J = 0) states of the CHD=CH radical. The states are labeled by irreducible representations of the C_s(M) molecular symmetry group and an assignment based on harmonic modes is also given. The wavenumbers are in cm^{-1}

i	$\tilde{\nu}_i$(a′)	Label	$\tilde{\nu}_i$(a″)	Label
1	0.0	*syn* GS	733.9	*anti* ν_9
2	29.0	*anti* GS	736.6	*syn* ν_9
3	633.7	*syn* ν_7	790.4	*syn* ν_8
4	646.4	*anti* ν_7	876.7	*anti* ν_8
5	901.6	*syn* ν_6	1343.7	*anti* $(\nu_7 + \nu_9)$
6	945.1	*anti* ν_6	1373.7	*syn* $(\nu_7 + \nu_9)$
7	1208.2	*syn* $2\nu_7$	1425.0	*syn* $(\nu_7 + \nu_8)$
8	1231.8	*syn* ν_5	1492.5	*anti* $(\nu_7 + \nu_8)$
9	1264.2	*anti* ν_5	1622.5	*syn* $(\nu_6 + \nu_9)$
10	1273.4	*anti* $(\nu_6 + \nu_7)$	1648.8	*anti* $(\nu_6 + \nu_9)$
11	1424.3	*syn* $(\nu_6 + \nu_7)$	1694.6	*anti* $(\nu_6 + \nu_8)$
12	1440.5	*anti* $2\nu_9$		
13	1463.6	*syn* $2\nu_9$		
14	1523.8	*syn* $(\nu_8 + \nu_9)$		
15	1535.8	*anti* $2\nu_7$		
16	1562.5	*syn* ν_4		
17	1578.6	*anti* $(\nu_8 + \nu_9)$		
18	1584.4	*syn* $2\nu_8$		
19	1593.2	*anti* ν_4		
20	1722.3	*anti* $2\nu_8$		

effective potential governing the tunneling motion. This effective asymmetry perturbs significantly the internal motions and causes mixing of the symmetric and antisymmetric ''unperturbed'' tunneling states and, in the end, compared to the other isotopologues studied, results in drastically different energy levels and splittings for CHD=CH. As can be rationalized *via* a simple two-state double-well tunneling model,[49,51] for the lowest states, when the effective energy difference between the two structures is larger than the tunneling splitting for the unperturbed case, the asymmetry of the two wells leads to localization of the delocalized unperturbed tunneling wave functions. The same model predicts that at higher energies, when the enhanced tunneling splittings become (much) larger than the asymmetry of the wells, delocalized wave functions and thus bistructural states[49,51] will again be observed.

Table 13 contains the computed vibrational states of CHD=CH, labeled according to the C_s(M) MS group. For illustration of the tunneling-switching behavior of CHD=CH, Fig. 5 provides density plots of the first 11 vibrational states of A' symmetry.

We can immediately observe in Fig. 5 that for CHD=CH the unperturbed delocalized GS pair is combined into *syn* and *anti* localized (unistructural[51]) states, with an energy separation as large as 30 cm^{-1}. Similarly, the ν_5 and ν_4 states (the latter is not shown) exhibit localized wave function densities along the C_αH rocking coordinate (ϑ_3), while also being split by about 30 cm^{-1}. All these states have small tunneling splittings in the parent molecule, CH_2=CH. Thus, they nicely represent the limiting case giving rise to unistructural states. States ν_6 and ν_7 of the parent are characterized by splittings comparable to the perturbation. Although these states are sort of localized, their splittings are no longer close to 30 cm^{-1}. The unperturbed splitting of states $2\nu_7$ and $\nu_6 + \nu_7$ is about 100 and 85 cm^{-1}, respectively, *i.e.*, considerably larger than the perturbation. In accordance with expectation, we can observe that the densities along the ϑ_3 coordinate are rather delocalized in these states and the splittings are substantial, 328 and 151 cm^{-1}, respectively.

In contrast to these nice tunneling switching examples following the expectation based on the two-state model, the ν_8 and ν_9 states of A″ symmetry (not shown), despite having small unperturbed splitting values and being localized, do not have the anticipated 30 cm^{-1} splitting, but rather 85 cm^{-1} and 3 cm^{-1}, respectively. This behavior suggests that to explain these splittings more than the two states must be used in the perturbation treatment.

Interestingly, the pronounced ν_6 and ν_7 interaction is also present in the CHD=CH isotopomer. We can see this in the density plots, which are almost identical for these two fundamentals, having a clear ν_6 mode structure even in the formally ν_7 states.

4 Conclusions

A large number of numerical results have been obtained as part of this study about the rovibrational states and the quantum dynamics of the following VR isotopologues: CH_2=CH, CH_2=CD, CD_2=CD, and CHD=CH. The most important findings of this study concerning the high-resolution spectroscopy of these species can be summarized as follows:

(1) Although several potential energy surfaces are available[36,39] corresponding to the ground electronic state, $\tilde{X}^2A'$, surface of the vinyl radical, the accuracy they provide is seemingly not yet sufficient for high-accuracy spectroscopic studies whose aim is to help decipher complex high-resolution experimental spectra.

(2) The complex nuclear dynamics of the different isotopologues of the vinyl radical depends strongly on the barrier hindering the C_αH rocking motion, leading to pronounced tunneling behavior. Therefore, the focal-point analysis (FPA) scheme was used in this study to determine an accurate value for the height of this barrier. The final FPA value is 1641(25) cm^{-1}, with a conservative uncertainty estimate.

(3) Both the ν_6 (formally CH_2 rock) and ν_7 (formally CH rock) modes contribute strongly to the tunneling dynamics of all the vinyl radical isotopologues studied except CH_2=CD. Thus, it seems that at least these two internal motions must be included in a meaningful model to describe tunneling dynamics of VR and its deuterated isotopologues. The necessity to include both rocking-type motions at the two ends of the molecule makes the dynamical behavior of VR unusual and thus interesting. The involvement of both rocking motions in the tunneling dynamics means that scrambling of all three protons may be facilitated by complex motions. Large tunneling splittings have been computed not only for the ''traditional'' tunneling mode, ν_7, but also for ν_6. The tunneling splittings of the ν_6 and ν_7 modes are more than 20 times the tunneling splitting of the ground state (for which very similar splittings have been computed and measured). Note that the ν_6 and ν_7 modes are strong mixtures of the two rocking internal motions in CH_2=CH even at the harmonic level.

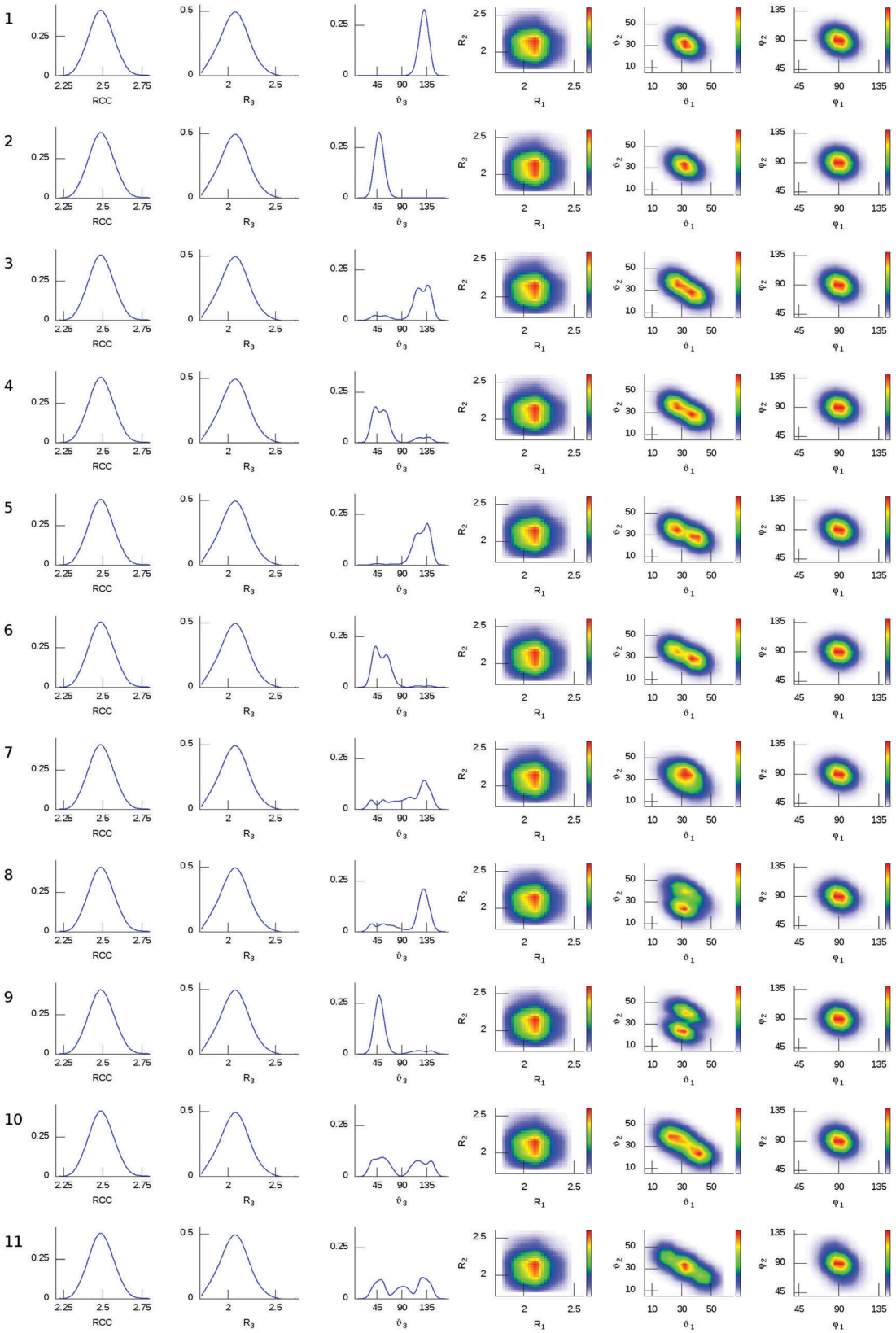

Fig. 5 D1RDM and D2RDM plots of the first 11 vibrational states of A′ symmetry of CHD═CH. Radial coordinates are in bohr, angular coordinates are in degrees.

(4) The vinyl radical, despite the extensive tunneling motion, behaves like a semirigid molecule as far as its overall rotational motion is considered. This is another somewhat surprising result of the present study, helping future experimental exploration of the high-resolution spectra of VR.

(5) There are a couple of notable discrepancies between the high-quality variational study of Yu *et al.*[40] and the present study, though they employ the same PES.[39] It is suggested that the present results represent more converged eigenstates corresponding to the same PES.

(6) The present study confirms the excellent high-resolution experimental investigations of Douberly *et al.*[23] concerning the fundamentals of CH_2═CH in the CH stretch region (ν_1, ν_2, and ν_3). The extensive results of matrix isolation studies[16] for ν_5 and ν_8 are also confirmed by the present investigation. The infrared diode laser kinetic spectroscopy study of Hirata *et al.*[11] of the $\nu_8^{\pm}$ fundamental is also fully supported. Based on the present investigation, corrections to the placement of ν_4 and ν_6 are proposed. We basically support the time-resolved IR emission spectroscopy[21] result of 1595(10) cm^{-1} for ν_4. The ν_6 fundamental should be around 991 cm^{-1}, with a large tunneling splitting of +14 cm^{-1}. Note also that none of the fundamentals of CH_2═CH proposed by a time-resolved FTIR emission spectroscopy study[13] are supported.

(7) Based on the high quality of the computed results for CH_2═CH, it is believed that the vibrational levels computed for the deuterated analogues, CH_2═CD, CD_2═CD, and CHD═CH, should have a comparably high level of accuracy. The same should hold for the tunneling splittings computed as part of this study.

(8) The asymmetrically substituted analogue, CHD═CH, is a nice new example of the tunneling switching phenomenon.[49–51] For CHD═CH the unperturbed delocalized ground-state pair is combined into *syn* and *anti* localized (unistructural) states, with an energy separation as large as 30 cm^{-1}, almost an order of magnitude larger than for the bistructural ground state of CH_2═CH. Some of the higher-lying vibrational states are again delocalized (bistructural), as expected when the splitting of the unperturbed states becomes (much) larger than the perturbation causing the effective asymmetry of the double-well potential.

The present study also offers some findings related to the variational computation of rovibrational states of molecules exhibiting complex internal motions, including tunneling. These results can be summarized as follows:

(1) Use of the symmetry-adapted version of the GENIUSH code[60] for the computation of vibrational eigenstates offers significant advantages. First, determination of a large number of vibrational eigenstates is considerably simpler this way than without consideration of symmetry. Second, symmetry labels, including parity, are provided straightforwardly by these computations, which is highly useful when trying to distinguish close-lying states.

(2) A contraction scheme,[66] whereby instead of solving the full-dimensional variational vibrational problem at once, first two subsystems (in the present case the bend and the stretch systems) are treated and then the partial solutions are used as elements of a reduced direct-product basis, works very well even for this system showing complex nuclear dynamics. It seems clear that one can save on the memory requirements of the computations, though CPU usage may not be significantly less than solving the full problem at once if accuracy is an issue and a large number of states needs to be computed.

(3) Plotting one- and two-mode reduced density matrices, in fact their diagonal elements, D1RDM and D2RDM, respectively, rather than producing wave function plots, seems to have clear advantages. The D1RDM and D2RDM formalisms seem to provide a semiautomatic way to assign labels to computed vibrational wave functions. Nevertheless, in problematic cases of strongly interacting modes a manual intervention still seems to be necessary.

It is hoped that the large number of accurate results obtained in this study will prompt further experimental (high-resolution spectroscopic) investigations on the isotopologues of VR and lead to an even more definitive understanding of the interesting but complex nuclear motions characteristic of this radical.

Conflicts of interest

There are no conflicts to declare.

Acknowledgements

AGC and CF gratefully acknowledge the financial support they received from NKFIH through grants K119658 and PD124699, respectively. Our research also received support from the grant VEKOP-2.3.2-16-2017-00014, supported by the European Union and the State of Hungary and co-financed by the European Regional Development Fund. Professor Yang is thanked for providing the NN-PES as well as for useful discussions concerning the use of this PES.

References

1 P. R. Westmoreland, A. M. Dean, J. B. Howard and J. P. Longwell, *J. Phys. Chem.*, 1989, **93**, 8171.
2 J. A. Miller, R. J. Kee and C. K. Westbrook, *Annu. Rev. Phys. Chem.*, 1990, **41**, 345.
3 R. K. Janev and D. Reiter, *Phys. Plasmas*, 2004, **11**, 780.
4 A. Fahr, P. S. Monks, L. J. Stief and A. H. Laufer, *Icarus*, 1995, **116**, 415.
5 R. W. Fessenden and R. H. Schuler, *J. Chem. Phys.*, 1963, **39**, 2147.
6 E. L. Cohran, F. J. Adrian and V. A. Bowers, *J. Chem. Phys.*, 1964, **40**, 213.
7 P. H. Kasai and E. B. Whipple, *J. Am. Chem. Soc.*, 1967, **89**, 1033.
8 P. H. Kasai, *J. Am. Chem. Soc.*, 1972, **94**, 5950.
9 H. E. Hunziker, H. Kneppe, A. D. McLean, P. Siegbahn and H. R. Wendt, *Can. J. Chem.*, 1983, **61**, 993.
10 R. A. Shepherd, T. J. Doyle and W. R. M. Graham, *J. Chem. Phys.*, 1988, **89**, 2738.

11 H. Kanamori, Y. Endo and E. Hirota, *J. Chem. Phys.*, 1990, **92**, 197.
12 D. Forney, M. Jacox and W. Thompson, *J. Mol. Spectrosc.*, 1995, **170**, 178.
13 L. Letendre, D.-K. Liu, C. D. Pibel, J. B. Halpern and H.-L. Dai, *J. Chem. Phys.*, 2000, **112**, 9209.
14 E. Kim and S. Yamamoto, *J. Chem. Phys.*, 2002, **116**, 10713.
15 K. Tanaka, M. Toshimitsu, K. Harada and T. Tanaka, *J. Chem. Phys.*, 2004, **120**, 3604.
16 H. Tanskanen, L. Khriachtchev, M. Räsänen, V. I. Feldman, F. F. Sukhov, A. Y. Orlov and D. A. Tyurin, *J. Chem. Phys.*, 2005, **123**, 064318.
17 A. Carvalho, G. Hancock and M. Saunders, *Phys. Chem. Chem. Phys.*, 2006, **8**, 4337.
18 F. Dong, M. Roberts and D. J. Nesbitt, *J. Chem. Phys.*, 2008, **128**, 044305.
19 Y.-J. Wu, M.-Y. Lin, B.-M. Cheng, H.-F. Chen and Y.-P. Lee, *J. Chem. Phys.*, 2008, **128**, 204509.
20 K. Tanaka, M. Hayashi, M. Ohtsuki, K. Harada and T. Tanaka, *J. Chem. Phys.*, 2009, **131**, 111101.
21 M. Nikow, M. J. Wilhelm and H.-L. Dai, *J. Phys. Chem. A*, 2009, **113**, 8857.
22 M. E. Jacox and W. E. Thompson, *J. Chem. Phys.*, 2011, **134**, 064321.
23 P. L. Raston, T. Liang and G. E. Douberly, *J. Chem. Phys.*, 2013, **138**, 174302.
24 M. Hayashi, K. Harada, R. Lavrich, T. Tanaka and K. Tanaka, *J. Chem. Phys.*, 2010, **133**, 154303.
25 L. B. Harding, *J. Am. Chem. Soc.*, 1981, **103**, 7469.
26 M. Dupuis and J. J. Wendoloski, *J. Chem. Phys.*, 1984, **80**, 5696.
27 M. N. Paddon-Row and J. A. Pople, *J. Phys. Chem.*, 1985, **89**, 2768.
28 L. A. Curtiss and J. A. Pople, *J. Chem. Phys.*, 1988, **88**, 7405.
29 J.-H. Wang, H.-C. Chang and Y.-T. Chen, *Chem. Phys.*, 1996, **206**, 43.
30 A. M. Mebel, Y.-T. Chen and S.-H. Lin, *Chem. Phys. Lett.*, 1997, **275**, 19.
31 K. A. Peterson and T. H. Dunning, Jr., *J. Chem. Phys.*, 1997, **106**, 4119.
32 K. W. Sattelmeyer and H. F. Schaefer III, *J. Chem. Phys.*, 2002, **117**, 7914.
33 A. R. Al Derzi, S. Fau and R. J. Bartlett, *J. Phys. Chem. A*, 2003, **107**, 6656.
34 G. V. Mil'nikov, T. Ishida and H. Nakamura, *J. Phys. Chem. A*, 2006, **110**, 5430.
35 D. J. Nesbitt and F. Dong, *Phys. Chem. Chem. Phys.*, 2008, **10**, 2113.
36 A. R. Sharma, B. J. Braams, S. Carter, B. C. Shepler and J. M. Bowman, *J. Chem. Phys.*, 2009, **130**, 174301.
37 E. Kamarchik, Y. Wang and J. Bowman, *J. Phys. Chem. A*, 2009, **113**, 7556.
38 A. R. Sharma, J. M. Bowman and D. J. Nesbitt, *J. Chem. Phys.*, 2012, **136**, 034305.
39 L. Chen, K. Shao, J. Chen, M. Yang and D. H. Zhang, *J. Chem. Phys.*, 2016, **144**, 194309.
40 H.-G. Yu, H. Song and M. Yang, *J. Chem. Phys.*, 2017, **146**, 224307.
41 A. Fahr and A. H. Laufer, *J. Phys. Chem.*, 1988, **92**, 7229.
42 A. Fahr, P. Hassanzadeh and D. B. Atkinson, *Chem. Phys.*, 1998, **236**, 43.
43 C. D. Pibel, A. McIlroy, C. A. Taatjes, S. Alfred, K. Patrick and J. B. Halpern, *J. Chem. Phys.*, 1998, **110**, 1841.
44 M. B. Pushkarsky, A. M. Mann, J. S. Yeston and C. B. Moore, *J. Chem. Phys.*, 2001, **115**, 10738.
45 M. Shahu, C.-H. Yang, C. D. Pibel, A. McIlroy, C. A. Taatjes and J. B. Halpern, *J. Chem. Phys.*, 2002, **116**, 8343.
46 G. Czakó, E. Mátyus and A. G. Császár, *J. Phys. Chem. A*, 2009, **113**, 11665.
47 I. Szabó, C. Fábri, G. Czakó, E. Mátyus and A. G. Császár, *J. Phys. Chem. A*, 2012, **116**, 4356.
48 P. L. Chapovsky and L. J. F. Hermans, *Annu. Rev. Phys. Chem.*, 1999, **50**, 315.
49 M. Quack, *Chem. Phys. Lett.*, 1986, **132**, 147.
50 S. Albert, P. Lerch, R. Prentner and M. Quack, *Angew. Chem., Int. Ed.*, 2013, **52**, 346.
51 S. Albert, Z. Chen, C. Fábri, P. Lerch, R. Prentner and M. Quack, *Mol. Phys.*, 2016, **114**, 2751.
52 E. R. Cohen, *J. Mol. Spectrosc.*, 1980, **79**, 496.
53 X. Huang, D. W. Schwenke and T. J. Lee, *J. Chem. Phys.*, 2011, **134**, 044321.
54 A. G. Császár and T. Furtenbacher, *Phys. Chem. Chem. Phys.*, 2016, **18**, 1092.
55 P. R. Bunker and P. Jensen, *Molecular Symmetry and Spectroscopy*, NRC Research Press, Ottawa, 2nd edn, 1998.
56 A. G. Császár, W. D. Allen and H. F. Schaefer III, *J. Chem. Phys.*, 1998, **108**, 9751.
57 A. G. Császár, W. D. Allen, Y. Yamaguchi and H. F. Schaefer, *Computational Molecular Spectroscopy*, Wiley, New York, 2000, pp. 15–68.
58 A. G. Császár, G. Tarczay, M. L. Leininger, O. L. Polyansky, J. Tennyson and W. D. Allen, *Spectroscopy from space*, Kluwer, Dordrecht, 2001, pp. 317–339.
59 I. M. B. Nielsen, C. L. Janssen, N. A. Burton and H. F. Schaefer, *J. Phys. Chem.*, 1992, **96**, 2490.
60 C. Fábri, M. Quack and A. G. Császár, *J. Chem. Phys.*, 2017, **147**, 134101.
61 E. Mátyus, G. Czakó and A. G. Császár, *J. Chem. Phys.*, 2009, **130**, 134112.
62 C. Fábri, E. Mátyus and A. G. Császár, *J. Chem. Phys.*, 2011, **134**, 074105.
63 J. C. Light and T. Carrington, Discrete-variable representations and their utilization, in *Advances in Chemical Physics*, John Wiley & Sons, Inc., 2007, pp. 263–310.
64 C. Lanczos, *J. Res. Natl. Bur. Stand.*, 1950, **45**, 255.
65 E. Mátyus, C. Fábri, T. Szidarovszky, G. Czakó, W. D. Allen and A. G. Császár, *J. Chem. Phys.*, 2010, **133**, 034113.
66 C. Fábri, R. Marquardt, A. G. Császár and M. Quack, *J. Chem. Phys.*, 2018, manuscript accepted for publication.
67 M. Yang, personal communication.
68 J. Echave and D. C. Clary, *Chem. Phys. Lett.*, 1992, **190**, 225.
69 H. Wei and T. Carrington Jr., *J. Chem. Phys.*, 1992, **97**, 3029.

70 V. Szalay, G. Czakó, A. Nagy, T. Furtenbacher and A. G. Császár, *J. Chem. Phys.*, 2003, **119**, 10512.
71 J. F. Stanton, J. Gauss, L. Cheng, M. E. Harding, D. A. Matthews and P. G. Szalay, second of two note CFOUR, a quantum chemical program package written by J. F. Stanton, J. Gauss, L. Cheng, M. E. Harding, D. A. Matthews, P. G. Szalay with contributions from A. A. Auer, R. J. Bartlett, U. Benedikt, C. Berger, D. E. Bernholdt, Y. J. Bomble, O. Christiansen, F. Engel, R. Faber, M. Heckert, O. Heun, M. Hilgenberg, C. Huber, T.-C. Jagau, D. Jonsson, J. Jusélius, T. Kirsch, K. Klein, W. J. Lauderdale, F. Lipparini, T. Metzroth, L. A. Mück, D. P. O'Neill, D. R. Price, E. Prochnow, C. Puzzarini, K. Ruud, F. Schiffmann, W. Schwalbach, C. Simmons, S. Stopkowicz, A. Tajti, J. Vázquez, F. Wang, J. D. Watts and the integral packages MOLECULE (J. Almlöf and P. R. Taylor), PROPS (P. R. Taylor), ABACUS (T. Helgaker, H. J. A. Jensen, P. Jørgensen, and J. Olsen), and ECP routines by A. V. Mitin and C. van Wüllen. For the current version, see http://www.cfour.de.
72 W. D. Allen and A. G. Császár, *J. Chem. Phys.*, 1993, **98**, 2983.
73 INTDER is a set of programs written by W. D. Allen and co-workers which performs various vibrational analysis and higher-order nonlinear transformations among force field representations.
74 W. D. Allen, A. G. Császár, V. Szalay and I. M. Mills, *Mol. Phys.*, 1998, **89**, 1213.
75 P. Pulay and F. Török, *Acta Chim. Hung.*, 1965, **44**, 287.
76 W. D. Allen, A. G. Császár and D. A. Horner, *J. Am. Chem. Soc.*, 1992, **114**, 6834.
77 R. D. Cowan and D. C. Griffin, *J. Opt. Soc. Am.*, 1976, **66**, 1010.
78 G. Tarczay, A. G. Császár, W. Klopper and H. M. Quiney, *Mol. Phys.*, 2001, **99**, 1769.
79 H. Sellers and P. Pulay, *Chem. Phys. Lett.*, 1984, **103**, 463.
80 Y. Yamaguchi, N. C. Handy and H. F. Schaefer III, *J. Chem. Phys.*, 1986, **84**, 4481.
81 MRCC, a quantum chemical program suite written by M. Kállay, Z. Rolik, J. Csontos, P. Nagy, G. Samu, D. Mester, J. Csóka, B. Szabó, I. Ladjánszki, L. Szegedy, B. Ladóczki, K. Petrov, M. Farkas, P. D. Mezei, and B. Hégely. See also Z. Rolik, L. Szegedy, I. Ladjánszki, B. Ladóczki, and M. Kállay, *J. Chem. Phys.*, 2013, **139**, 094105, as well as: http://www.mrcc.hu.
82 K. A. Peterson, D. E. Woon and T. H. Dunning, *J. Chem. Phys.*, 1994, **100**, 7410.
83 A. Karton and J. M. L. Martin, *Theor. Chem. Acc.*, 2006, **115**, 330.
84 A. Halkier, T. Helgaker, P. Jorgensen, W. Klopper, H. Koch, J. Olsen and A. K. Wilson, *Chem. Phys. Lett.*, 1998, **286**, 243.
85 A. G. Császár, E. Mátyus, T. Szidarovszky, L. Lorenzo, N. F. Zobov, S. V. Shirin, O. L. Polyansky and J. Tennyson, *J. Quant. Spectrosc. Radiat. Transfer*, 2010, **111**, 1043.
86 D. A. Sadovskii, N. G. Fulton, J. R. Henderson, J. Tennyson and B. I. Zhilinskii, *J. Chem. Phys.*, 1993, **99**, 906.
87 J. Sarka and A. G. Császár, *J. Chem. Phys.*, 2016, **144**, 154309.
88 J. Šmydke and A. G. Császár, *Mol. Phys.*, 2019, manuscript accepted for publication.
89 F. Tamassia, E. Cané, L. Fusina and G. Di Lonardo, *Phys. Chem. Chem. Phys.*, 2016, **18**, 1937.
90 J. Demaison, J. Cosléou, R. Bocquet and A. G. Lesarri, *J. Mol. Spectrosc.*, 1994, **167**, 400.
91 J. M. Colmont, G. Wlodarczak, D. Priem, H. S. P. Müller, E. H. Tien, R. J. Richards and M. C. L. Gerry, *J. Mol. Spectrosc.*, 1997, **181**, 330.
92 G. Tasi, M. Szöri and A. G. Császár, *J. Phys. Chem. A*, 2005, **109**, 4824.
93 N. C. Craig, P. Groner and D. C. McKean, *J. Phys. Chem. A*, 2006, **110**, 7461.

